



CENTRE FOR AUSTRALIAN REGOLITH STUDIES

**WEATHERING AT THE TRIAL HILL
TIN MINE - QUEENSLAND**

Volume I

by

I.D.M. Robertson

**Centre for Australian Regolith Studies
Occasional Publication No. 1**

August, 1990

THE AUSTRALIAN NATIONAL UNIVERSITY
CANBERRA

**WEATHERING AT THE TRIAL HILL
TIN MINE - QUEENSLAND**
(VOLUME I)

by

I.D.M. ROBERTSON

CENTRE FOR AUSTRALIAN REGOLITH STUDIES
OCCASIONAL PUBLICATION No 1

August, 1990

**CENTRE FOR AUSTRALIAN REGOLITH STUDIES,
Australian National University
University of Canberra**

© Centre for Australian Regolith Studies

ISBN 0 858 89438 6

First published 1990
Reprinted 1994

This work is copyright. Apart from any fair dealings for the purposes of study, research, criticism or review as permitted under the Copyright Act, no part may be reproduced by any process without written permission. Copyright is the responsibility of the Co-Directors of the Centre for Australian Regolith Studies (Australian National University, PO Box 4 Canberra, ACT 0200; and University of Canberra, PO Box 1 Belconnen, ACT 2616).

PREFACE

This is the first Occasional Publication of the Centre for Australian Regolith Studies. This Centre was established at the beginning of 1988, as a joint venture between the Australian National University and the University of Canberra. The Centre is based in the Department of Geology at the ANU and is part of the Graduate School of Quaternary and Regolith Studies. The Centre has three functions: to provide a focus for regolith research in Canberra, where there are many organisations involved in regolith-related work; to develop an integrated Australian regolith research program; and to offer training in regolith studies.

STAFF: Directors: Dr Tony Eggleton (ANU) and Dr Graham Taylor (UC). Research Fellows: Dr M. Le Gleuher, Dr F. Ghassemi; (half time, from CRES).

This publication contains the results of a rock weathering study at the Trial Hill Tin Mine, in northern Queensland. Initially this study, together with a similar study at Kerrimenge, in Papua-New Guinea, was designed to investigate the differences between kaolinite produced by hydrothermal activity and kaolinite generated by weathering. All samples were initially collected by staff of Rennison Goldfields Exploration Pty. Ltd., and those from Trial Hill, in particular, by Mr. Kevin Robinson. A considerable amount of investigation was carried out on these samples before the Trial Hill Tin Mine was visited by the author.

As it turned out neither area was suitable for a study of hydrothermal kaolinite. The clays and their fabrics, generated by weathering, particularly at Trial Hill, were worthy of a detailed investigation. This Occasional Publication contains the results of this research and largely covers the local geology and also the weathering of the complete rock suite at Trial Hill.

A large amount of otherwise unpublished microprobe data of various mineral phases, including clay pseudomorphs after recognisable precursor minerals, are included in an extensive appendix (Appendix 1). Some of this data have been displayed using a novel stereographic plotting method (Appendix 2). These were plotted using a computer program modified from a routine developed by Lenthall *et al* (1974), and the program, which is available for the Macintosh and IBM PC environments, may be obtained from the author (IDMR). To view these plots, a standard mirror stereoscope is required.

A more specialised investigation was also carried out at Trial Hill. This was on the transformation of muscovite to kaolinite and kaolinite to halloysite and provides, in particular, new evidence for the mechanism for growth of halloysite spirals. This is being published and a draft is included as Appendix 3.

R. A. Eggleton
Director

TABLE OF CONTENTS

| | Page |
|---|------|
| ABSTRACT | 4 |
| INTRODUCTION | 5 |
| GEOLOGY | 5 |
| Regional Geology and Geomorphology | 5 |
| Granitic Basement | 5 |
| Tin-bearing Leads | 8 |
| PETROGRAPHY OF COLLECTED MATERIAL | 11 |
| Pink Granite | 11 |
| Kaolinitic Granite | 18 |
| Debris-flow Sediment | 22 |
| Clay Sediment | 24 |
| COMPARISONS OF MINERAL PHASES | 27 |
| Primary Mineralogy of Specimen MJ8 and Specimen MJ10 (Pink Granite) | 27 |
| K-feldspars of Kaolinised Granites: Specimen MJ7 and MJ9 | 30 |
| Coarse-grained Kaolinites and Micas of the Granite and Kaolinised Granite | 31 |
| Kaolinites of the Debris-flow Sediments | 32 |
| Kaolinites after Plagioclase | 33 |
| Coarse- and Fine-grained Kaolinites | 33 |
| A TEM EXAMINATION OF COMPONENTS OF SPECIMEN MJ6 | 34 |
| GEOCHEMISTRY | 38 |
| Methods | 38 |
| Major Elements | 39 |
| Trace Elements | 39 |
| Tin Geochemistry | 45 |
| INTERPRETATION | 45 |
| ACKNOWLEDGEMENTS | 46 |
| REFERENCES | 47 |

WEATHERING AT THE TRIAL HILL TIN MINE - QUEENSLAND

¹I.D.M. Robertson

ABSTRACT

Cassiterite has been mined at Trial Hill from a Pliocene river channel, cut into deeply-weathered granite. The base of the channel has been filled with a lower sequence of at least three debris-flows, overlain by false-bedded fluvial gravels. It was initially suggested that the river channel locally followed and covered a zone of hydrothermal kaolinisation and greisenisation in the granite.

The granite consists of quartz, albite, flecked with muscovite, and microcline perthite, with minor chloritised biotite. Weathering has altered the albite to a mixture of kaolinite, halloysite and muscovite. The K-feldspar shows some alteration but, in many places, it is fresh. However its perthitic albite component has been completely altered to a mesh of halloysite tubes. Quartz is unchanged. Accordion structures of mixed muscovite and kaolinite have grown in the granitic saprolite.

TEM investigation of the alteration of kaolinite to halloysite in the plagioclase pseudomorph showed that, on hydration to halloysite, the clay crystal curls. Parts of the crystal, which contain remnants of kaolinite, retain local rigidity and linearity, resulting in a polygonal spiral of halloysite, much like a rolled newspaper. The most common forms are pentagons and hexagons.

Comparison of the major and minor element geochemistry of the fresh granite and the kaolinised granite show differences that are consistent with weathering when expressed on a mass per unit volume basis. There has been the expected loss of some Si and Fe as well as Ca, Na, K, Rb and Sr, with corresponding gains in H⁺, Al, and V. Ti, Mn, Ba, Pb, Sn and Zr have remained relatively stable. The geochemistry of the debris-flow sediments is remarkably similar to that of the kaolinised granite. Though the debris-flow sediments are slightly enriched in Zr, Sn, and V, and depleted in Ba, Sr, K, Rb and Pb, this is consistent with derivation of the sediment from the most intensely weathered top of the granite saprolite.

The hypothetical zone of hydrothermal kaolinisation under the river channel has not been supported by field, petrographic, mineralogical or geochemical evidence. Only weathering phenomena have been found and the sediments appear to have been stripped from an already deeply weathered granitic terrain. Weathering no doubt continued since sedimentation.

¹Present address:- Division of Exploration Geoscience, CSIRO, Private Bag PO Wembley, WA 6014. Australia.

INTRODUCTION

A reported kaolin-rich, tin-bearing, funnel-like feature at the Trial Hill Tin Mine in central Queensland was suggested as a source of hydrothermally generated kaolinites for comparison with kaolinites generated by weathering. The exposure, as described by an exploration geologist during a brief field visit, was a kaolin funnel within a pink, fine- to medium-grained biotite granite. Greisenisation was said to have occurred along a fault and tin (cassiterite) was being worked from kaolinitic gravels formed by redeposition of altered granitic material, preserved under a basaltic capping.

GEOLOGY

Regional Geology and Geomorphology

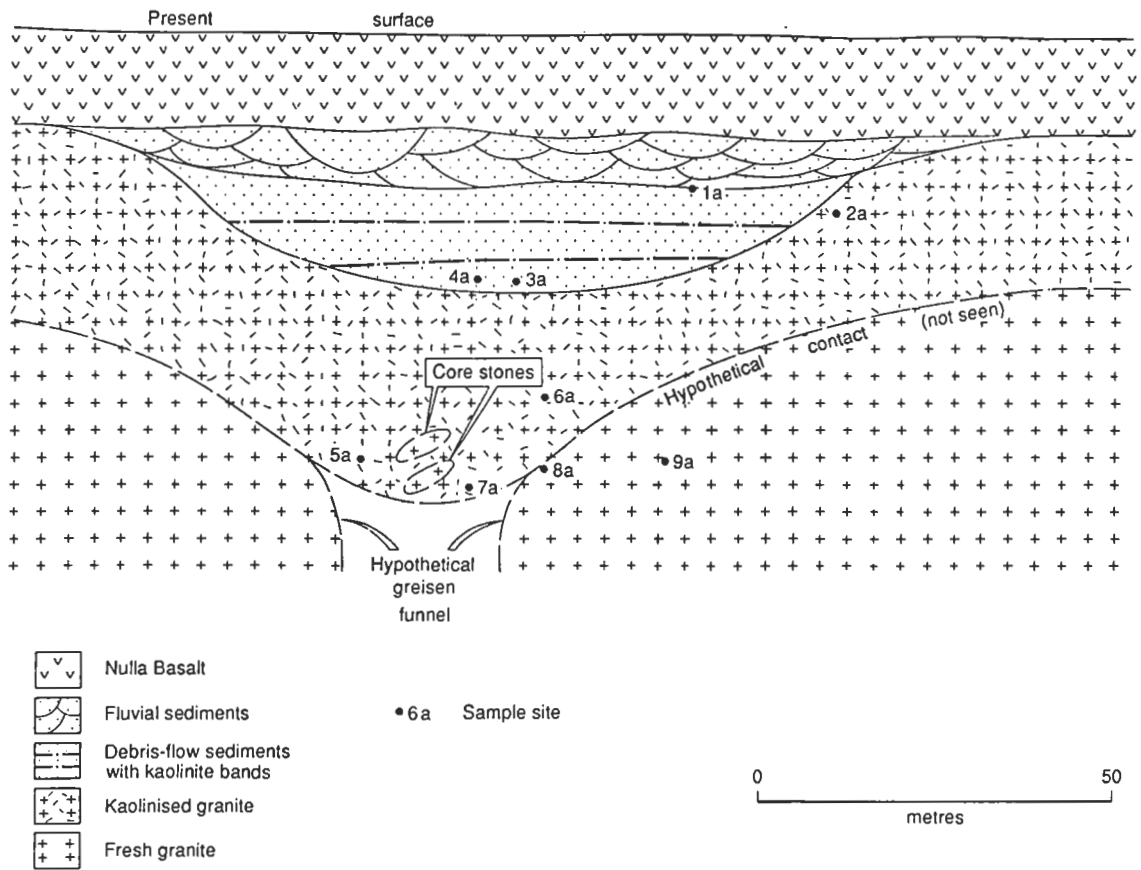
The field area was visited by the author for three days during 1986 and the local geology and erosional environment were studied in detail. The Trial Hill Tin Mine (located at 145° 51' 26" E; 18° 59' 11" S) is an open-cut operation in cassiterite-bearing Pliocene fluvial gravels. These lie upon the Upper Carboniferous Owenee Granite and are capped by the Pliocene-Pleistocene Nulla Olivine Basalt. The BMR 1:250,000 map sheets Ingham and Townsville refer (see Wyatt *et al*, 1970). Several remnants of an old erosion surface lie at a height of 720-740 m, some 9 km to the north-east of the mine and are marked by lateritic cappings on granite. Here extensive mottled zone material has been brought to the surface by termites (Plate 2F). These laterite surfaces seem equivalent to the 'older', generally red, laterite profile of Wyatt *et al* (1970) and underlie the Campaspe Beds. The Trial Hill Tin Mine lies at an altitude of about 600 m and consists of a small valley, cut in a kaolinised granitic basement, filled with cassiterite-bearing debris-flow and fluvial gravels (Plate 1A) which are, in part, capped by basalt (Figure 1, Plate 1A).

Granitic Basement

The granitic basement is a pink, medium-grained biotite granite, here referred to as the 'pink' granite, which is deeply kaolinised below laterite surfaces and below the tin-bearing leads. In places, as about 3 km south of Trial Hill, the granite is cut by numerous parallel to sub-parallel black quartz veins (Plate 2A). It is thought that these are the source of the tin. The black quartz veins are accompanied by localised kaolinisation, probably related to easier ingress of groundwater along the vein margin. This black quartz is identical to some of the quartz seen in the lead gravels (Plate 2B), the more abundant grey quartz in the gravel was probably derived from the granite itself. The primary tin grade was probably too low for mining but fluvial concentration of the heavy cassiterite has given rise to richer deposits suitable for smallworking.

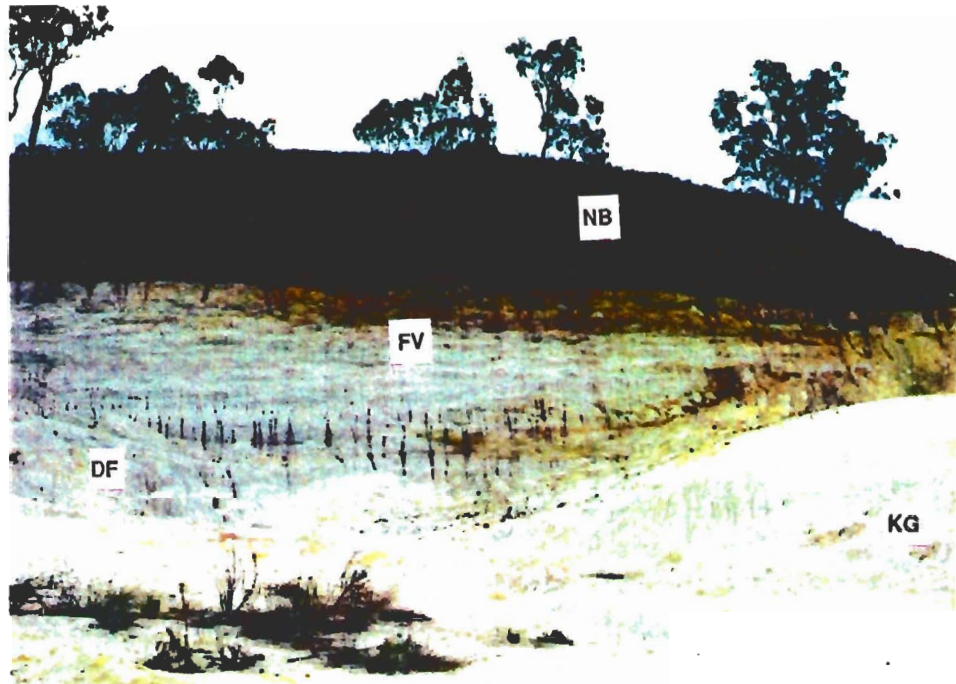
The floor of the deepest exposed parts of the open cut at the Trial Hill Mine is a pink, very slightly weathered granite. This is overlain by a white to pale-cream kaolinised granite of similar fabric and grain size (Plate 2C). The contact between the two was not seen, though evidence was found of remnants (corestones) of the pink granite within the kaolinised granite (Plate 2D). The central part of the fluvial

FIGURE 1

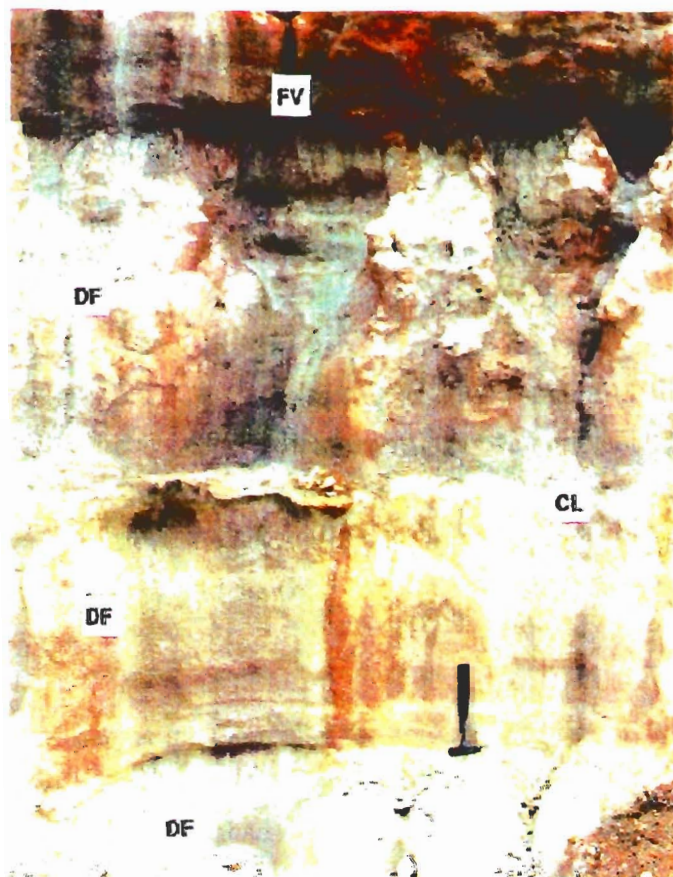


Sketch cross section of the Central Open Cut at the Trial Hill Tin Mine, showing major rock units and sample sites. Refer also to Plate 1A.

PLATE 1



A. Central Open-Cut at Trial Hill Tin Mine. Fluvial sediments (FV) overlie debris-flow sediments (DF) which in turn rest on a basement of kaolinised granite (KG). The whole is capped by Nulla Basalt (NB).



B. Southern Open Cut. Detail of Plate 2E. Three layers of debris-flow sediments (DF) are each capped by thin clay layers (CL). The base of the false-bedded fluvial sediments (FV) is shown at the top.

trough was said to be underlain by a kaolinised greisen. This critical exposure was covered by mine debris at the time of the field visit. The kaolinised granite is cut by several kaolinite veins (probably original felsic dykes), sub parallel to the main axis of the lead. The kaolinised granite is found in several localities in contact with, and overlain by, kaolinitic debris-flow and fluvial sediments.

Tin-bearing Leads

There are two contrasted parts to the leads; lower, massive and upper, well-layered sediments. The lower sediments are several metres in thickness, medium-grained, massive and rather structureless (Plate 2E). They lie on kaolinised granite and are also composed of quartz and kaolinite. This sedimentary unit can be eight metres or more in thickness and comprises several layers, interspersed by very thin argillaceous layers (Plate 1 B). There is no significant erosion of the lower layer by any succeeding layer.

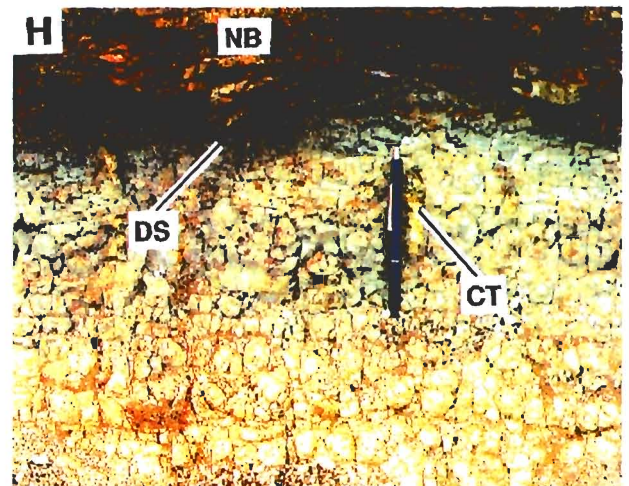
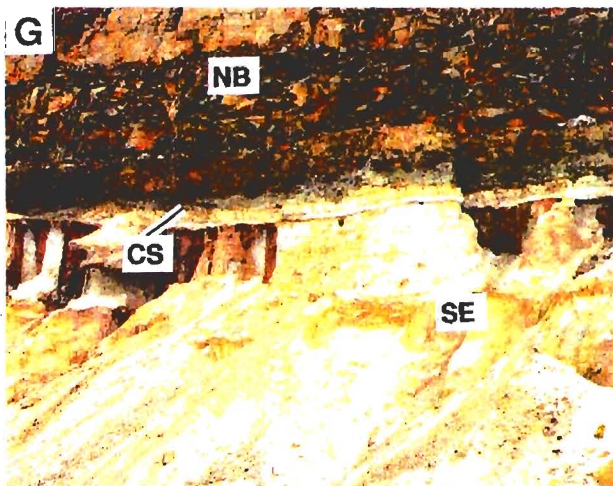
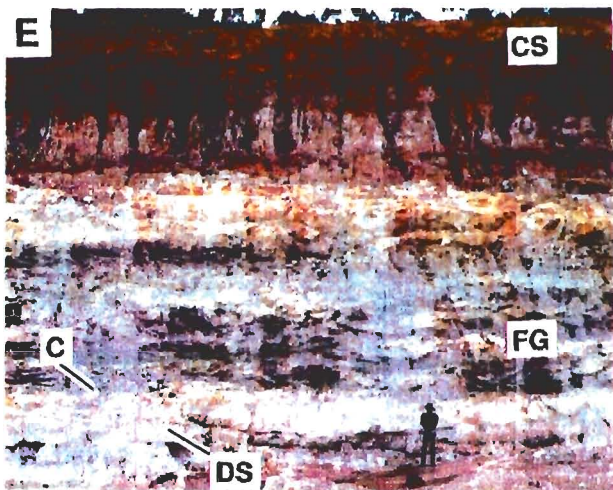
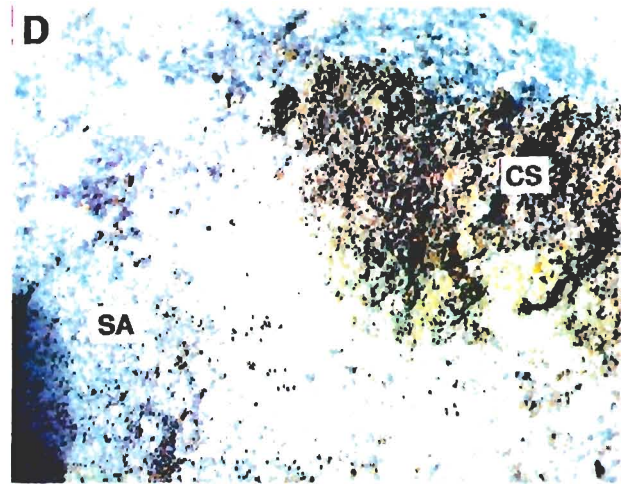
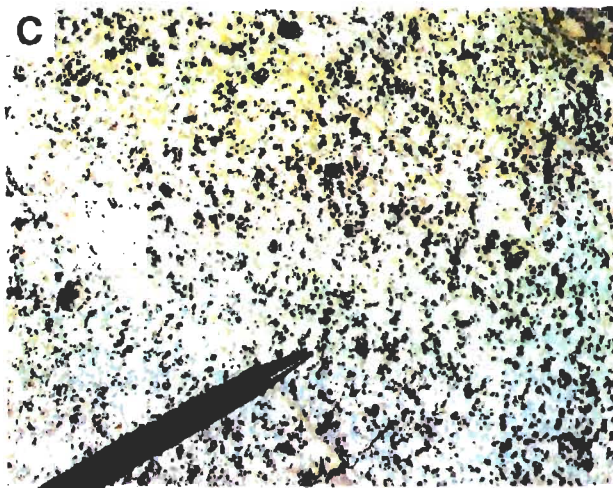
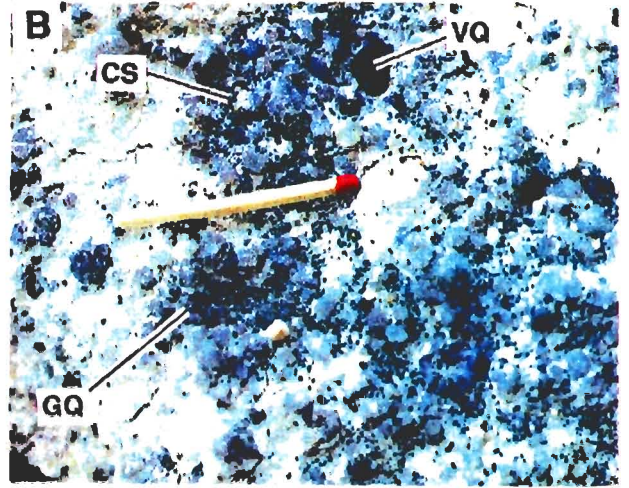
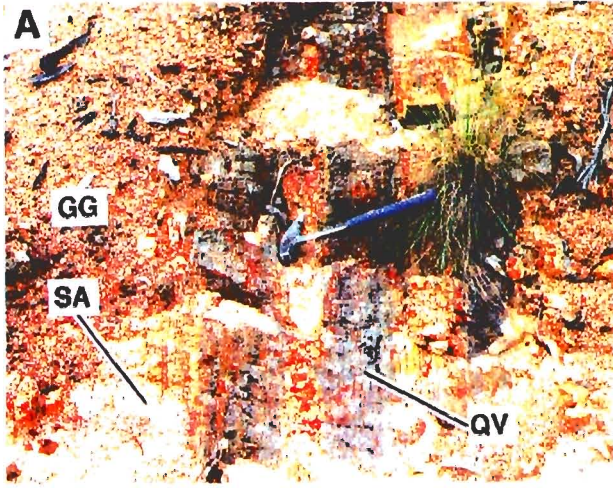
This poorly-sorted sediment is considered to have been deposited very rapidly from a debris-flow by reduction in transport velocity of a viscous sediment-rich fluid, the sediment having been locally stripped from the kaolinised granite. This material has all the features of a mud- or debris-flow, poor sorting, matrix-supported clasts, no apparent erosion of the underlying surface (Reineck and Singh, 1980). The thin but persistent, intercalated clay layers were probably deposited slowly from muddy water, overlying the debris-flow, after it had come to rest.

The upper, laminated part is a composite lens of fluvial gravels, about 9 m thick in the channel centre. The gravel layers within this lens are themselves lensoid, each only 0.05-1.0 m in thickness, consisting of coarse, angular to sub-rounded gravels of 2-20 mm grain size, consisting of grey to black quartz. These fine upward into a sandstone and some are capped by a thin clay band. False bedding is common. Hydrated iron oxides have permeated and cemented some of the upper parts of the fluvial deposits, accentuating their structure. At the margins, these fluvial gravels lap directly upon kaolinised granite and in the centre upon the debris-flow sediments. The sequence is capped by the Nulla olivine basalt in the Central open-cut (Plates 1A and 2G). The top of the sedimentary sequence, just below the basalt, is a layer of about 300 mm of clay or clay soil. The upper part has been darkened and indurated by the hot basalt and contains narrow pipe-like features, some 10 mm in diameter, interpreted as steam vents, now filled with a yellowish clay (Plate 2H). The fluvial deposits are not covered by basalt in the northern and southern open-cuts but are capped by an armouring of white silcrete. This silcrete is rich in blue opaline silica.

The gravels were first worked just before the turn of the century. They were accessed from small shafts and concentrations of tin were removed from small drives and stopes in what must have been very unstable, dangerous ground. Some of these drives and stopes are now exposed in the sides of the northern open-cut. The style of the deposit is analogous to the Au and Pt leads at Fifield (NSW), the Au and diamondiferous leads at Ayerley Mountain (NSW) and the deep Au leads around Ballarat (VIC).

PLATE 2

- A. Dark grey to black quartz vein (QV) cutting partly kaolinised granitic saprock (SA), partly masked by granitic grus (GG). About 3 km south of Trial Hill Tin Mine.
- B. Small granules of cassiterite (CS) with larger, pale grey grains of granitic quartz (GQ) and dark grey vein quartz (VQ) in white kaolinite matrix of fluvial gravel facies of tin lead. Trial Hill Tin Mine.
- C. Kaolinised granite saprolite, containing granular pale grey quartz grains and white kaolinite. Central open-cut, Trial Hill Tin Mine.
- D. Corestones of pink, crumbly, slightly weathered granite (CS), set in granitic saprolite (SA). Central open-cut, Trial Hill Tin Mine, adjacent to C.
- E. The upper, approximately horizontal contact (C) of the debris-flow sediments (DS) and the cross-bedded fluvial gravels (FG) lies just above the standing field assistant. The upper part of the profile is masked by colluvial soil (CS).
- F. Termitaria of red soil on the upper part of the laterite profile (mottled zone) 9 km north-east of the Trial Hill Tin Mine.
- G. The top part of the sedimentary sequence (SE), overlain by what appears to be a clay soil (CS), capped by the Nulla Basalt (NB).
- H. Detail of the top of the soil and the base of the basalt (NB). The upper part of the soil has been darkened (DS) and indurated and contains clay-filled tubes (CT), interpreted as steam vents.



PETROGRAPHY OF COLLECTED MATERIAL

Pink Granite

Two granite samples are described, one of 'fresh' pink granite (Specimen MJ8) and the other from the edge of the 'greisen funnel' (Specimen MJ10) and their locations are given in Figure 1.

Site 9a (Specimen MJ8) is within the 'fresh' granite. It is a pink, very slightly weathered biotite granite, consisting of pink, fresh K-feldspar, creamy, rather altered plagioclase, glassy, grey quartz, partly chloritised biotite and minor muscovite. Bulk XRD analysis indicated kaolinite and illite as well.

The rock in thin section consists of quartz, plagioclase and microcline perthite, with minor biotite. The biotite has been variably chloritised (Appendix 1, Tables 1A/1 and 1A/2) and shows colours varying from brown to deep green, variable pleochroism and a wide range of birefringence (Plate 3A). The probable crystallisation sequence is plagioclase -> K-feldspar -> quartz.

The quartz crystals shows strain lamellae normal to the c axis (Plate 3B), very similar in appearance to the tartan twinning of microcline (Hobbs, 1968; Morrison-Smith *et al*, 1976). An SEM examination of sonified samples of quartz showed small pits of variable shape, about 3 µm across, which are probably fluid inclusion pockets (Plate 4C). The plagioclase occurs as sericitised, equant to stumpy, subhedral, lath-like grains 0.5-3.0 mm in size, which tend to occur in clusters, showing albite and pericline twins. It is clouded and carries inclusions of fine-grained sericite and coarser-grained muscovite patches 0.05 mm in size. The plagioclase is albite ($Ab_{97.5} An_{1.8} Or_{0.7}$; Appendix 1, Table 1A/3), is lightly sericitised (Plate 3C) and has a gross fabric analogous to the fabric of one variety of kaolinite, seen in the kaolinised granite. The K-feldspar has formed large anhedral crystals, which enclose the plagioclase, and is a vein and patch perthite (Plate 3D). Its fabric is accentuated by clouding of the K-feldspar which has a composition of $Ab_{4.3} An_{0.0} Or_{95.8}$ (Appendix 1, Table 1A/4: Analyses 8.24; 8.22). An SEM examination of both feldspars showed feldspar cleavage and very little evidence of etching. There are brown radiation damage haloes in the chloritised biotite and some apatite occurs in the mica cleavage. There is also a trace of epidote and the plagioclase contains small flakes of muscovite. None of this is atypical of a granite.

Though there are no apparent primary opaque minerals, there are some black and brown iron oxides associated with small cracks along which weathering has penetrated. One of these was analysed and consists of MnO (35.35%) with minor SiO₂ (2.2%), MgO (2.14%), FeO (1.81%), CaO (1.49%) and traces of Na₂O and K₂O.

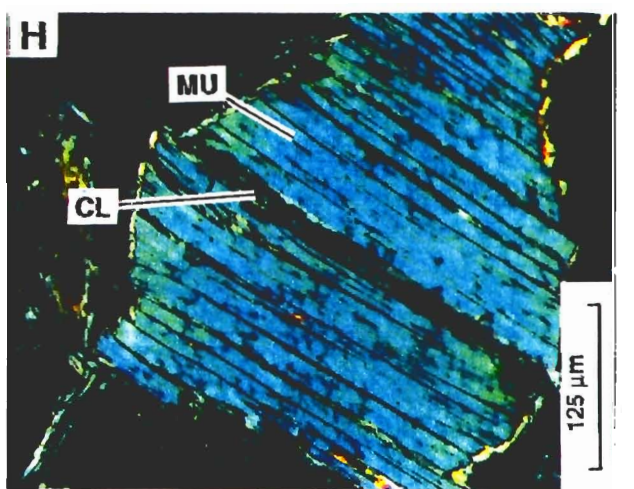
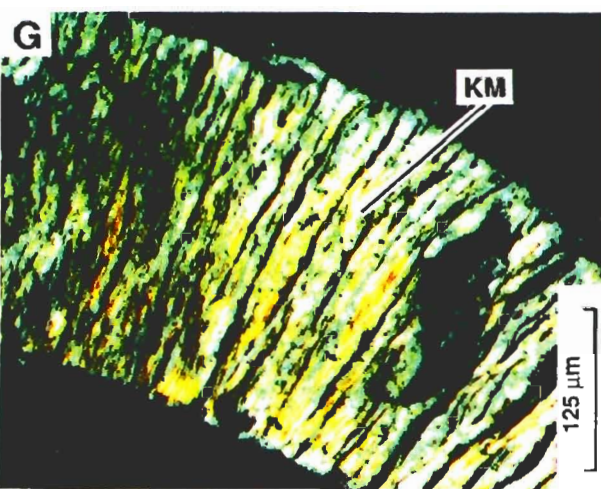
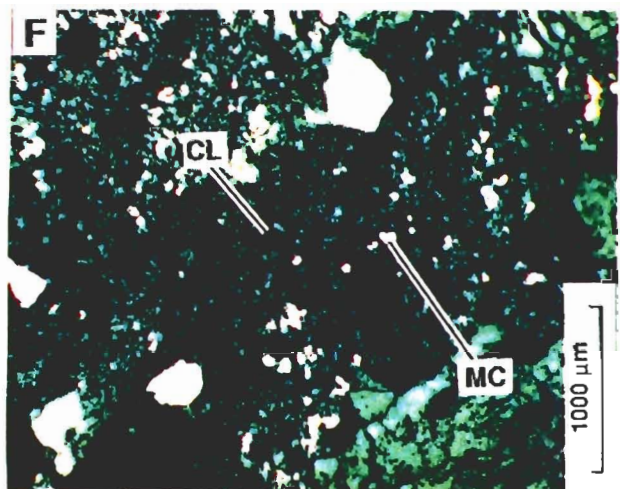
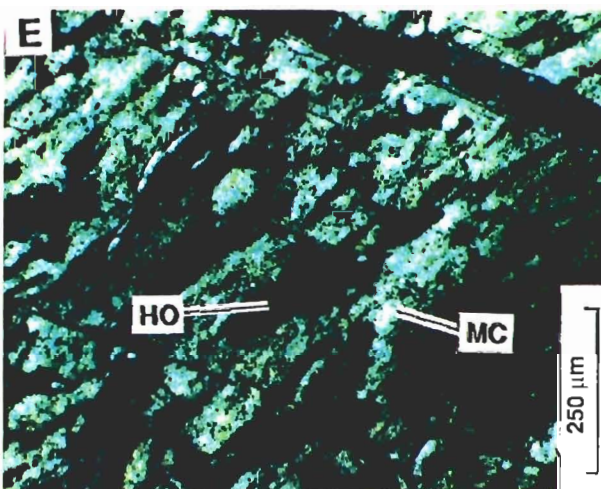
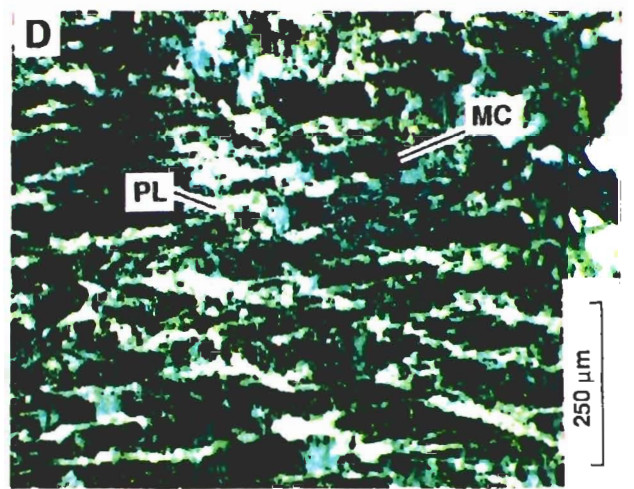
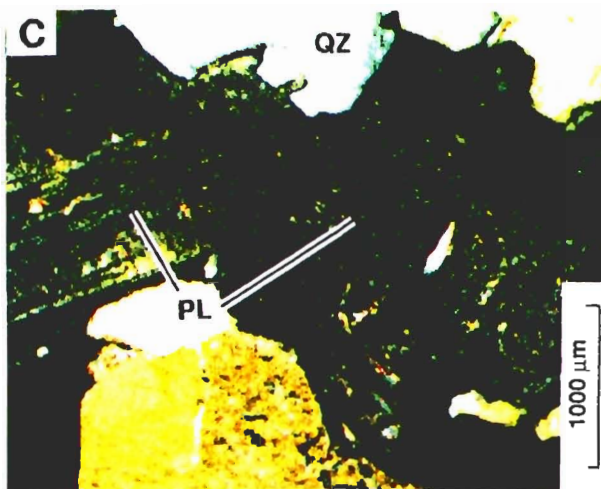
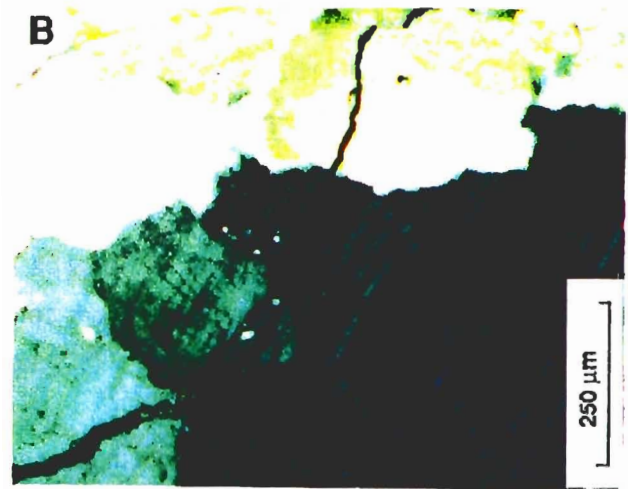
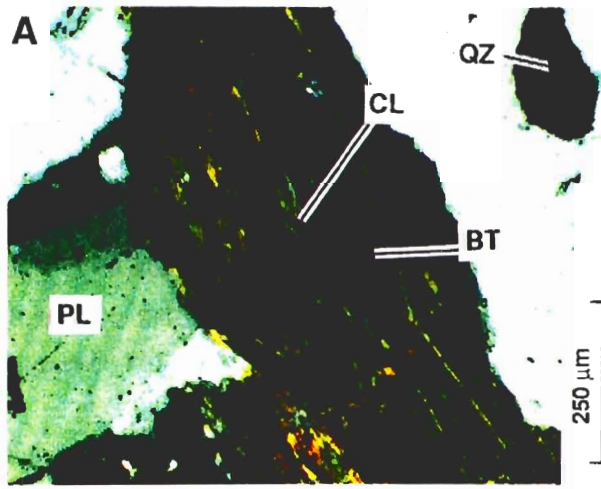
PLATE 3

Fresh Granite

- A. Partly chloritised biotite, showing alternating layers of greenish chlorite (CL) and brown biotite (BT) set in fresh plagioclase (PL) and quartz (QZ). Specimen MJ8, Site 9a. Crossed polarizers.
- B. Strain lamellae in quartz showing a cross-hatch structure. Specimen MJ8, Site 9a. Crossed polarizers.
- C. Slightly sericitised plagioclase (PL), showing mica inclusions, with quartz (QZ) in fresh granite. Specimen MJ8. Site 9a. Compare with F. Crossed polarizers.
- D. Slightly turbid but otherwise fresh microcline crystal (MC) containing clear, fresh, vein perthitic plagioclase (PL). Specimen MJ8. Site 9a. Compare with E. Crossed polarizers.

Kaolinised Granite

- E. Weathered microcline crystal showing fresh K-feldspar (MC) but the perthitic plagioclase has been completely converted to halloysite (HO). Compare with D. Specimen MJ9. Site 7a. Crossed polarizers.
- F. Very fine-grained low birefringent kaolinite (CL), flecked with patches of mixed kaolinite and mica (MC), which together form a pseudomorph after sericitised plagioclase. Compare with C. Specimen MJ9. Site 7a. Crossed polarizers.
- G. Accordion structure of mixed kaolinite and mica (KM). The birefringence varies from first order yellow to grey. Specimen MJ9. Site 7a. Crossed polarizers.
- H. Interleaved but discrete fresh muscovite (MU) and clay (CL). The muscovite has been split open by the clay. Specimen MJ9. Site 7a.



Site 8a (Specimen MJ10) is from the triple contact of the 'fresh' granite, the kaolinitic granite and the 'greisen funnel'. Visually it is a pink, slightly weathered granite consisting of pink K-feldspar, cream plagioclase and glassy, grey quartz. The only mafic mineral was biotite, now largely altered to chlorite. Bulk XRD analysis indicated some smectite and illite as well. All the minerals are flecked with spots (0.10-0.05 mm in size) of what is probably an hydrated manganese oxide. This granite is similar to Specimen MJ8 but appears to be slightly less weathered.

In thin section it consists of quartz, sericitised plagioclase and much microcline perthite. The K-feldspar is a vein and patch perthite, the microcline being intensely clouded brown and the plagioclase component being left largely unaffected, accentuating the perthite structure. There seems to be some crystallographic control to the orientation of the muscovite within the plagioclase. Muscovite does not however generally occur in the perthite.

The separate plagioclase phase is albite An_{3,3} (Appendix 1 ,Table 1A/5). It is clouded and contains sericite and flecks of muscovite. In places some of the plagioclase crystals have been partly altered to kaolinite, where the plagioclase structure disappears, to be replaced by a mass of very low-birefringent material. A detailed examination of the weathered plagioclase by SEM showed rounded, cellular encrustations of smectite (honeycomb-cornflake fabric, 1 µm) set with a few rods of halloysite (Plates 4E and F), attached to the plagioclase substrate. The etched plagioclase surface shows a number of fine-scale, parallel cleavage cracks spaced at 0.5-1.0 µm (Plate 4A). As etching proceeds, the cracks widen to a parallel boxwork to which small crystals (3 µm) of clay cling (Plate 4B). Similar smectite honeycomb fabrics were found on etched microcline.

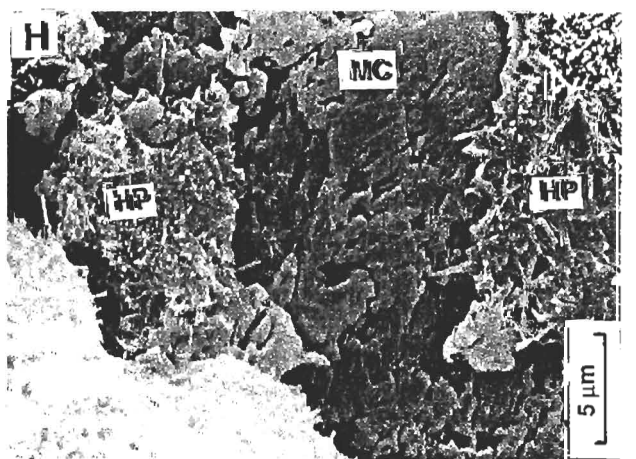
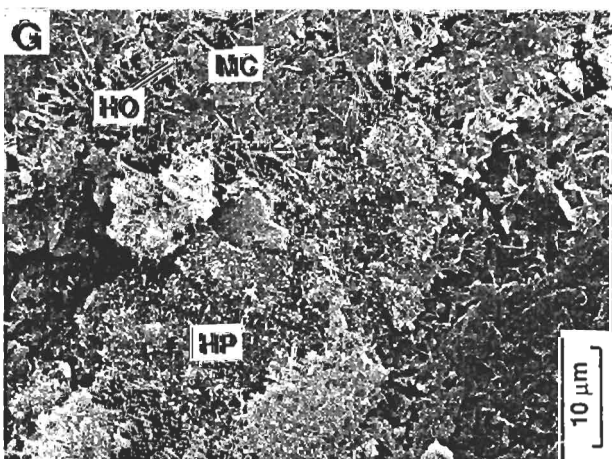
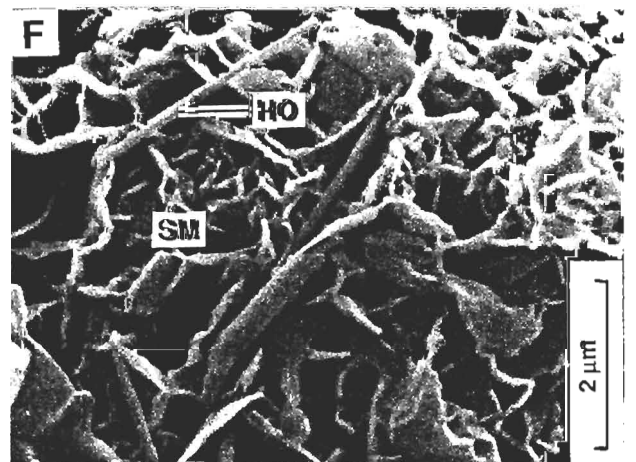
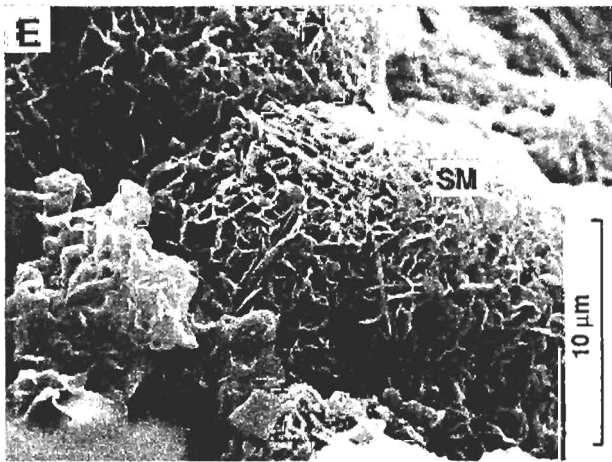
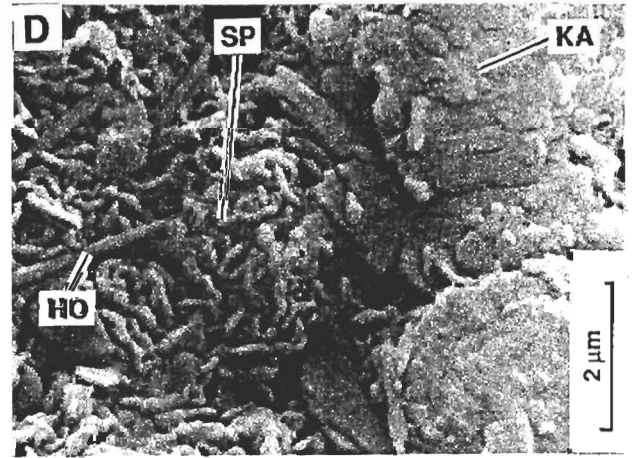
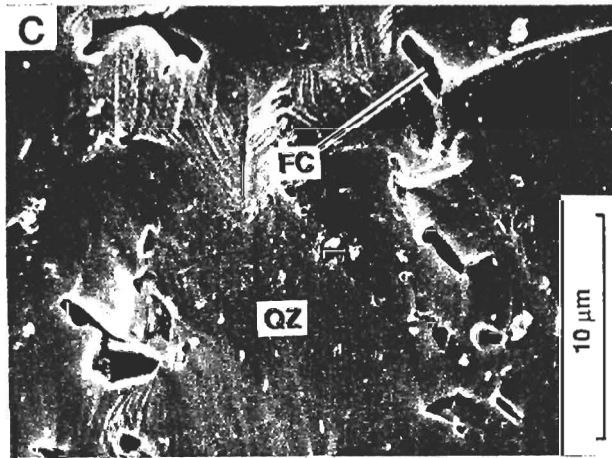
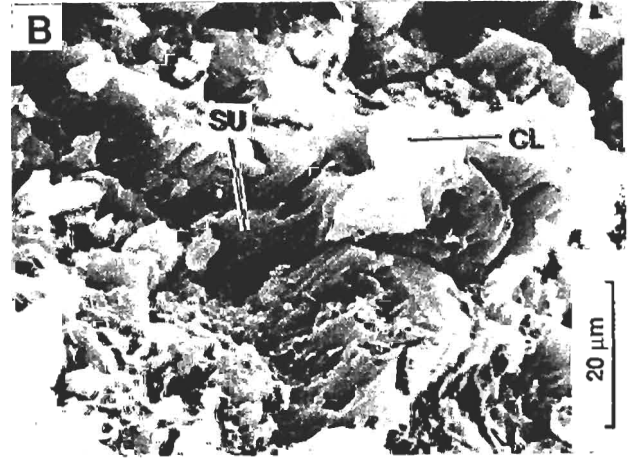
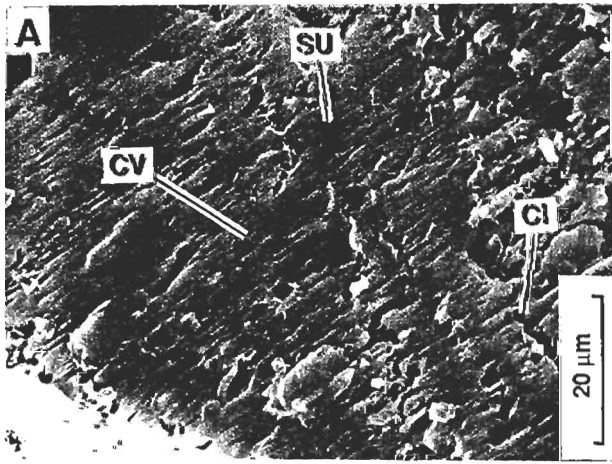
TABLE 1

FELDSPARS OF MJ10 AND MJ8

| | <i>10Plag</i> | <i>8 Plag</i> | <i>10Plag.per</i> | <i>8Plag.per</i> | <i>10Kspar</i> | <i>8Kspar</i> | <i>2s Error</i> |
|-------|---------------|---------------|-------------------|------------------|----------------|---------------|-----------------|
| Si | 2.956 | 2.948 | 2.982 | 2.973 | 2.979 | 2.975 | 0.018 |
| Al | 1.053 | 1.047 | 1.035 | 1.030 | 1.019 | 1.024 | 0.008 |
| Fe+3 | 0.0 | 0.001 | 0.000 | 0.003 | 0.006 | 0.013 | 0.010 |
| ΣTet | 4.009 | 3.996 | 4.017 | 4.006 | 4.004 | 4.012 | - |
| Mg | 0.000 | 0.001 | 0.000 | 0.000 | 0.001 | 0.002 | 0.001 |
| Ca | 0.033 | 0.018 | 0.018 | 0.011 | 0.000 | 0.000 | 0.004 |
| Na | 0.936 | 0.972 | 0.924 | 0.930 | 0.045 | 0.043 | 0.022 |
| K | 0.014 | 0.007 | 0.009 | 0.061 | 0.970 | 0.959 | 0.012 |
| Σ "X" | 0.983 | 0.998 | 0.951 | 1.002 | 1.016 | 1.004 | - |
| Ab | 95.3 | 97.5 | 97.2 | 92.9 | 4.5 | 4.3 | 2.2 |
| An | 3.3 | 1.8 | 1.9 | 1.1 | 0.0 | 0.0 | 0.7 |
| Or | 1.4 | 0.7 | 1.0 | 6.1 | 95.5 | 95.8 | 2.0 |
| n | 9 | 3 | 1 | 2 | 8 | 2 | - |

PLATE 4

- A. Etched plagioclase surface (SU) showing a number of fine-scale cleavages (CV) which have been fretted out, particularly where cleavages intersect (CI).
- B. A more intensely etched plagioclase surface (SU) with small clinging clay particles (CL).
- C. The broken surface of a quartz crystal (QZ) showing small fluid inclusion pockets (FC).
- D. Flakes of kaolinite (KA) and rods of halloysite (HO), coated with a very thin manganiferous layer, together with a spaghetti-like probable manganese mineral (SP) or manganese-coated smectite.
- E. Rounded, cellular encrustations of smectite (SM), showing a typical cornflake fabric, on plagioclase.
- F. Detail of E showing smectite (SM) and a few rods of halloysite (HO).
- G,H. Weathered microcline perthite. An etched microcline surface (MC), with a few attached halloysite rods (HO) and patches of original perthitic plagioclase, now completely altered to a mass of halloysite rods (HP).



The rock is poorer in mafic minerals than Specimen MJ8 and only contains a small amount of chloritised biotite and some muscovite. An SEM examination of the chlorite showed small lenses of ilmenite or rutile in the cleavage. Small pockets in the chlorite were found to contain smectite and halloysite.

Microprobe analysis of the perthite revealed a cloudy microcline ($Or_{95.5} Ab_{4.5} An_{0.0}$) and a clear plagioclase component ($Or_{1.0} Ab_{97.2} An_{1.9}$). A few alkali feldspars of intermediate composition were recorded but these seem to be due to overlap of perthite phases in the mineral volume of X-ray emission. The data are presented in Appendix 1, Tables 1A/5, 1A/6 and 1A/7. The separate plagioclase phase, as distinct from the plagioclase of the perthite, is clear, well twinned and has a mean composition of $Or_{1.4} Ab_{95.3} An_{3.4}$ with scatter within 1.5% An. The mean structural formulae of these feldspars are given in Table 1.

The muscovite was also analysed. The average structural formula is given in Table 2 (see also Appendix 1, Table 1A/8, analyses 10.51-10.60). Both of these relatively fresh granite specimens had no features inconsistent with slight weathering.

TABLE 2
MUSCOVITE OF MJ10

| | <i>Average Muscovite 2sError</i> | |
|--------------|----------------------------------|-------|
| Si | 3.222 | 0.067 |
| Al | 0.778 | 0.067 |
| Al | 1.720 | 0.295 |
| Ti | 0.005 | 0.005 |
| Fe+2 | 0.231 | 0.195 |
| Mn | 0.010 | 0.009 |
| Mg | 0.116 | 0.113 |
| Σ Oct | 2.082 | - |
| Large Cation | | |
| Ca | 0.002 | 0.003 |
| Na | 0.032 | 0.015 |
| K | 0.849 | 0.136 |
| Σ L.C. | 0.883 | - |
| n | 10 | - |

The manganiferous black spots on Specimen MJ10 were examined using both XRD and the SEM. Some small flakes of this material were scraped off quartz so as to avoid, as much as possible, contamination by the substrate. Repeated attempts to obtain a satisfactory diffraction pattern (Debye-Scherrer) were frustrated. Both Cr and Fe radiation were used and even Cr radiation in a helium atmosphere. The best that could be obtained (Cr-He) was a very faint and diffuse diffraction at about 7.3 Å. Other faint

diffractions were identified as those of substrate contamination (feldspar and kaolinite). The SEM study was more helpful. A manganese EDXA map of the area confirmed a concentration of manganese. On closer examination, the manganiferous material was seen to have a lace-like appearance (Plate 4D). At high magnification, three phases were found. Rough, hexagonal flakes, about 3 μm across, appear to be kaolinite, coated by a manganiferous material. Though the Si/Al ratio is about correct for kaolinite, the peaks for these elements are dominated by a very strong manganese peak. Small rod-like structures of about 2 x 0.3 μm appear to be halloysite. Their chemistry appears to be similar to the kaolinite plates (as far as may be determined considering the area of X ray emission). A spaghetti-like mass of small vermiform structures (1 x 0.2 μm), which is as abundant or more abundant than the kaolinite, constitutes the third phase. This phase appears to be absent where manganese is absent. It may however not be a manganese mineral itself but could be manganese-coated smectite. The whole area could have had an amorphous manganiferous coating. A crack containing a manganese mineral in Specimen MJ8 was examined by microprobe (see above).

Kaolinitic Granite

Four samples of kaolinitic granite were collected at various levels in the profile and at various distances from the 'greisen funnel'.

A white kaolinitic granite (Site 2a, Specimen MJ11), high in the profile, immediately underlies the layered gravels. The grain size and fabric is similar to that of the pink granite. There are no preserved mafic minerals. Quartz, which occurs as anhedral, strained grains (0.5-2.0 mm) is the only completely unaltered mineral. Anhedral K-feldspar, showing twin structures and a slightly undulose extinction is all that remains of the perthite. The plagioclase component of the perthite has been converted entirely to extremely fine-grained clay. Another dominant clay phase, pseudomorphing the separate plagioclase phase, consists of a mass of fine-grained (0.005 mm), low birefringent kaolinite, set with clusters, larger flakes, books and distorted stacks of a more birefringent (yellow to red) kaolinite-muscovite mixture. These fine-grained kaolinites after plagioclase were investigated by microprobe (Appendix 1, Table 1A/9; Analyses 11.52-11.61). These mixed minerals are rich in iron and potassium, indicating admixture of muscovite as sericite, which was too fine grained to be resolved by the optical microscope or microprobe.

Muscovite-kaolinite intergrowths occur as patches 1.0-2.0 mm in size throughout the slide. In places lenses of weak grey birefringent clay may be seen penetrating strongly birefringent muscovite sheets. These have also been analysed by microprobe (Appendix 1, Table 1A/10; Analyses 11.39-11.51).

It is significant that the fabric and mineralogy of this rock is indistinguishable from those of the kaolinitised rocks of the 'greisen funnel'. If hydrothermal alteration had taken place then some mineralogical and/or fabric differences would have been expected.

A coarse-grained, white kaolinitic granite, from near the edge of the 'greisen funnel' (Site 6a, Specimen

MJ7) contains grey quartz and intensely kaolinised feldspars. Bulk XRD indicates a trace of illite. There are no mafic minerals. Though all the minerals, apart from quartz and K-feldspar, have been altered, this rock preserves a granitic fabric. The quartz is glassy and has a similar grain size and fabric to the quartz of the pink granites of Specimen MJ8 and Specimen MJ10. The K-feldspar is preserved and shows cleavage but is preferentially clouded with ultra-fine kaolinite. The K-feldspar has a mean composition of $Ab_{5.1} An_{0.1} Or_{94.9}$ (See Table 3; Appendix 1, Table 1A/11) but the plagioclase phase of the perthite is completely altered to clay.

The other kaolinite phase completely pseudomorphs a separate plagioclase phase. It consists mostly of a mat of fine-grained kaolinite (0.005 mm) which is set with patches of a coarser grained kaolinite (0.01-0.06 mm) which is more birefringent (white to yellow). The fine-grained kaolinites were examined by microprobe (Appendix 1, Table 1A/12, Analyses 7.14-7.25).

TABLE3
K-FELDSPARS OF MJ7

| | <i>Mean</i> | <i>Std Dev</i> |
|------------------|-------------|----------------|
| Si | 3.092 | 0.017 |
| Al | 1.042 | 0.005 |
| Fe ⁺³ | 0.001 | 0.002 |
| ΣTet | 4.135 | - |
| Mg | 0.000 | - |
| Ca | 0.000 | - |
| Na | 0.026 | 0.008 |
| K | 0.476 | 0.072 |
| Ti | 0.000 | - |
| Mn | 0.000 | - |
| Σ"X" | 0.502 | - |
| Ab | 5.1 | 1.0 |
| An | 0.1 | 0.2 |
| Or | 94.9 | 1.1 |

TABLE4
COMPARISON OF FINE-GRAINED KAOLINITES
OF MJ7 AND MJ11

| | MJ7 | | MJ11 | | <i>t</i> |
|------------------|-------------|----------------|-------------|----------------|----------|
| | <i>Mean</i> | <i>Std Dev</i> | <i>Mean</i> | <i>Std Dev</i> | |
| Si | 4.095 | 0.026 | 4.100 | 0.033 | 0.379 |
| Al | 3.774 | 0.041 | 3.698 | 0.050 | -3.735* |
| Fe ⁺² | 0.036 | 0.005 | 0.122 | 0.015 | 17.788* |
| Mg | 0.066 | 0.009 | 0.053 | 0.010 | -3.058* |
| Ca | 0.024 | 0.003 | 0.027 | 0.005 | 1.656 |
| Na | 0.007 | 0.002 | 0.007 | 0.002 | 0.000 |
| K | 0.037 | 0.005 | 0.094 | 0.032 | 5.799* |
| n | 12 | | 10 | | |

Critical value of *t* is ± 2.09 at 95% confidence level

When compared to similar kaolinites of Specimen MJ11, they are enriched in Al and Mg and relatively depleted in Fe, and K (Table 4). Some patches contain layers of highly birefringent muscovite, interleaved with kaolinite. The kaolinite penetrates the mica along its cleavage. The coarse-grained, more birefringent kaolinite-mica phase occurs as patches, some with bow-tie structures, and distorted stacks. It has been analysed by microprobe (Appendix 1, Table 1A/13, Analyses 7.26-7.37).

Both biotite and chlorite are absent. A very few globular grains of possible magnetite occur. Where small intergranular cracks intersect, these magnetite grains have been degraded to brown, hydrous iron oxides which stain the fine-grained kaolinite.

Site 7a (Specimen MJ9) is from the centre of the 'greisen funnel', near its upper contact with the kaolinitic granite. Visually there are a variety of kaolinite fabrics, from white, very fine-grained to pale, yellow-green and slightly micaceous.

Though all the minerals, apart from quartz and K-feldspar, have been altered, this rock still has a granitic fabric in thin section. The quartz is glassy and has a similar grain size and fabric to the quartz of the pink granites of Specimen MJ8 and Specimen MJ10. The plagioclase has now been altered to a very fine-grained kaolinite with a grain size of 0.002-0.006 mm. The K-feldspar, which is brown and clouded, shows Carlsbad twinning. Only the K-feldspar component of the original perthite remains, the plagioclase component having been converted to extremely fine-grained clay with a very low birefringence (Plate 3E). The K-feldspar has a composition of $Or_{97.6} Ab_{2.4} An_{0.0}$ (Appendix 1, Table 1A/14, analyses 9.14-9.18). Some of the K-feldspar is preferentially clouded with ultra-fine kaolinite .

The plagioclase component of the perthite has been converted entirely to a clay with an average structural formula as given in column 1 of Table 5 (see also Appendix 1, Table 1A/15, analyses 9.19-9.31). The separate plagioclase phase is not present but has been preserved as a slightly coarser-grained kaolinite with a low (grey-brown) birefringence (Plate 3F). This kaolinite phase has a rather varied grain size (<0.01-0.1 mm), appears to be interstitial to the other phases and has an average structural formula as illustrated in column 3 of Table 5 (see also Appendix 1, Table 1 A/16, Analyses 9.33-9.34). Comparison of the composition of the clay from plagioclase of plagioclase perthite and that from the separate plagioclase phase, indicates the clay derived from the plagioclase of the perthite is relatively rich in Al, Fe and Na and poor in Si, Ti, Mg, Ca and K compared to the equivalent clay from the plagioclase.

TABLE 5

MJ9
STRUCTURAL FORMULAE OF KAOLINITES
DERIVED FROM VARIOUS PHASES

| | Original Phase | | | | t |
|------------------|-----------------|-------------------|-------------------|--------------|---------|
| | <i>Perthite</i> | <i>Plag S.Dev</i> | <i>Plag Phase</i> | <i>S.Dev</i> | |
| Si | 4.136 | 0.084 | 4.259 | 0.006 | 1.792 |
| Al | 3.716 | 0.126 | 3.451 | 0.004 | -2.575* |
| Ti | 0.001 | 0.001 | 0.009 | 0.001 | 8.485* |
| Fe ⁺² | 0.064 | 0.032 | 0.109 | 0.010 | 1.695 |
| Mn | 0.000 | 0.000 | 0.000 | 0.000 | - |
| Mg | 0.044 | 0.013 | 0.098 | 0.003 | 5.043* |
| Ca | 0.024 | 0.004 | 0.058 | 0.029 | 2.419 |
| Na | 0.005 | 0.002 | 0.007 | 0.000 | 1.225 |
| K | 0.037 | 0.022 | 0.075 | 0.004 | 2.104 |
| n | 6 | | 2 | | |

Critical value for t is ± 2.45 at 95% confidence

TABLE 6

MJ6 AND 9
MUSCOVITE STRUCTURAL FORMULAE

| | <i>MJ6</i> | <i>MJ9</i> |
|------------------|------------|------------|
| Si | 3.142 | 3.210 |
| Al | 0.858 | 0.790 |
| Al | 2.082 | 1.713 |
| Ti | 0.000 | 0.005 |
| Fe ⁺² | 0.080 | 0.288 |
| Mn | 0.000 | 0.013 |
| Mg | 0.018 | 0.085 |
| Ca | 0.003 | 0.000 |
| Na | 0.013 | 0.025 |
| K | 0.396 | 0.837 |
| n | 3 | 2 |

Patches of coarse-grained clay, with a high (yellow-white) birefringence, forms distorted stacks (Plate 3G) and books and in places grades into muscovite with high second order blue-green birefringence. Some of the muscovite sheets are separated by thin wedges of clay (Plate 3H). Microprobe analyses of this clay are given in Appendix 1, Table 1A/17, Analyses 9.25-9.29. The micas have structural formulae illustrated in Table 6 and are muscovites (see also Appendix 1, Table 18, Analyses 9.23-9.24). Both biotite and chlorite are absent.

An SEM examination of this material shows an open mesh of plates of kaolinite (3 μm) set with randomly oriented rods of halloysite (1-3 μm long by 0.1 μm wide). Occasional tepee structures are seen. The halloysite rods do not have a round cross section but show flat or relatively flat planes parallel to their long

axes but further detail is limited by the resolution of the SEM. Many of the halloysite rods are attached to and lie flat upon plates of kaolinite. See Figure 1 F of Appendix 3.

Site 5a (Specimen MJ6) is from within the 'greisen funnel'. Visually it is a white, coarse-grained, intensely kaolinised granite. Bulk XRD shows it consists of quartz and kaolinite with a small amount of illite. The quartz is glassy and the kaolinite very fine-grained. In places the kaolinite has been stained yellow-brown by iron oxides. In places K-feldspar remains, showing cleavage surfaces and there are a few yellowish-green 'mica' patches.

The rock in thin section consists of large, composite grains of angular and in places sutured, strained quartz (0.4-4.0 mm in size) and irregular remnants of K-feldspar, set in a complex kaolinitic groundmass. The irregular grains of K-feldspar still retain twinning and a hint of perthitic structures, though their extinction is rather undulose and they seem to be divided into domains separated by zones of intense kaolinisation. An SEM examination of the altered microcline revealed an open mesh of kaolinite crystals (2-3 μm) and randomly oriented halloysite rods. As before, the halloysite rods are not round in cross section but have planar faces parallel to their long axes. In many instances the halloysite rods are found lying upon the kaolinite plates and appear to be partly fused with them. The resolution required to gather further information is beyond the capability of the SEM. The overall fabric of the altered perthite is seen in Appendix 3, Figure 1 E. Here the K-feldspar is deeply etched along cleavage planes and shows a delicate lace-like structure. A vermiform mesh of randomly oriented halloysite crystals, 3 μm in length, meandering in the etched feldspar, pseudomorphs the plagioclase phase of the perthite. See also Plates 4 G and H.

The separate plagioclase appears to have completely altered to a clay which consists of a fine-grained and a coarse-grained phase. The fine-grained phase (0.01 mm) forms patches 0.5-4.0 mm in size with a sutured fabric and grey birefringence. This has been analysed by microprobe (Appendix 1, Table 1A/19, Analyses 6.2-6.13). These kaolinites are slightly siliceous but are Ti-free. This phase is set, to a variable extent, with a coarser-grained kaolinite phase (0.05-0.20 mm), which forms distorted stacks, books and mats 0.05-0.30 mm in size, and has a white to yellowish birefringence. In places the mineral becomes more platy and the birefringence increases to second order blue-green (see also Appendix 1, Table 1A/20, Analyses 6.1-6.12). Here there seem to be discrete kaolinite and muscovite phases present. In other places the yellow-white birefringent kaolinite occurs as patches, books and distorted stacks up to 1.0 mm in size. Parts of the kaolinite fabric have been clouded by ultrafine kaolinite.

This rock is very similar to Specimen MJ9 of Site 7a. XRD of one of the book-like patches revealed kaolinite and smectite with minor quartz. Bulk XRD indicated a trace of illite. This particular sample has been intensively examined by TEM (see below).

Debris-flow Sediment

Two samples of debris-flow sediment were collected. One is white (Specimen MJ3/13) and the other

mottled with iron oxides (Specimen MJ5).

Site 3a (Specimen MJ3/13) is from the base of the debris-flow sediments. The sample is a medium-grained, clastic sediment, consisting of quartz and kaolinite, possibly with a little illite. The quartz is angular and shard-like, the groundmass is fine-grained kaolinite. Mafic minerals are absent.

In thin section (Specimen MJ3) it consists of shard-like, single, strained quartz grains 0.2-1.4 mm in size, set in a relatively coarse-grained groundmass of kaolinite and sparse, smaller, shard-like quartz. The kaolinite of the matrix has a dark grey birefringence, though it is set with a few flakes of micaceous kaolinite with a white or yellowish birefringence. The latter is probably a mixture of muscovite and kaolinite. A few patches of the matrix have been clouded by ultrafine kaolinite (seen as white patches in 45° illumination).

This rock is almost monomictic. Apart from quartz, the only other clasts are very rare fragments of an extremely fine-grained kaolinite rock. These were probably derived by fragmentation of the top fine-grained kaolinite layer of an underlying debris-flow or are fragments of weathered granitic kaolinite. Though a few quartz grains show re-entrant boundaries, this is not universal, so it seems that the kaolinitic matrix of the sediment has not corroded the quartz and corrosion probably occurred in the parent rock. The angular nature of the quartz indicates little clast wear and probably a very short transport distance. There are no mafic minerals at all.

Site 4a (Specimen MJ5) is at the base of the gravels. It consists of debris-flow material, very like Specimen MJ3/13 but the kaolinite is mottled with pink iron oxides. Quartz and kaolinite are the dominant minerals.

In thin section this rock consists of angular, shard-like quartz (0.2-2.4 mm in size), set in relatively coarse-grained (0.02 mm) kaolinite, with a flakey fabric, and sparse, fine-grained, shard-like quartz. The quartz is in singular grains and shows strain lamellae and some re-entrant grain boundaries. Some quartz grains contain inclusions of fresh, unaltered muscovite. There are rare clasts of kaolinitic material. The kaolinite groundmass, which contains a few micaceous flakes with a relatively high birefringence, has been clouded by ultra-fine kaolinite in patches, and both have been stained by red-brown iron oxides. There are no mafic minerals at all.

The stained and unstained kaolinites of the matrix were investigated by microprobe. The results are presented in Appendix 1. Table 1A/21 (Analyses 5.29-5.40) are of the unstained kaolinitic matrix and Appendix 1, Table 1A/22 (Analyses 5.41-5.52) are of the stained kaolinitic matrix. There is the expected relationship between the intensity of the red-brown colouration and the iron content (see Appendix 1, Table 1A/22). Deep red-stained kaolinites are shown in Analyses 5.46 and 5.52 (both 2.66% FeO). These Fe contents are significantly higher than the general level for the red-stained kaolinites (1.0-1.5% FeO) and 0.96% FeO for a very pale brown stained kaolinite.

TABLE 7
STAINED AND UNSTAINED KAOLINITES
OF THE MATRIX OF MJ15

| | Unstained | | Stained Red | | <i>t</i> |
|----|-------------|--------------|-------------|--------------|----------|
| | <i>Mean</i> | <i>S.Dev</i> | <i>Mean</i> | <i>S.Dev</i> | |
| Si | 3.909 | 0.015 | 3.879 | 0.027 | -3.221* |
| Al | 4.036 | 0.021 | 4.018 | 0.013 | -2.417* |
| Ti | 0.016 | 0.013 | 0.012 | 0.003 | -0.994 |
| Fe | 0.044 | 0.005 | 0.139 | 0.047 | 6.666* |
| Mg | 0.016 | 0.003 | 0.016 | 0.003 | 0.000 |
| Ca | 0.011 | 0.001 | 0.012 | 0.006 | 0.545 |
| Na | 0.009 | 0.003 | 0.015 | 0.004 | -3.980* |
| K | 0.045 | 0.026 | 0.038 | 0.008 | -0.853 |
| n | 12 | | 12 | | |

Critical value for *t* at 95% confidence is ± 2.07

Mean structural formulae of these kaolinites are presented in Table 7. Comparison of the two data sets indicates that the stained variety is significantly depleted in Si, Al and Na and very strongly enriched in Fe at the 95% confidence limit. This is well illustrated on the Si-Fe-Al ternary diagram (Figure 2) and on the Si-Al-Fe-Na plot (Appendix 2, Figure 2A/1) where their constant Si/Al ratio is well demonstrated. The unstained kaolinites show a trend of varying Na at a constant Si/Al ratio. The stained kaolinites show a trend towards Fe from this group. All the kaolinites lie on a distinct plane defined by the fixed Si/Al ratio, by Fe and Na.

These analyses conform quite well to the 1:1 Si:Al ratio of kaolinite and are not enriched in silica but they contain significant K and Ti. All the fabric and mineralogical evidence is not inconsistent with weathering and sedimentation.

Clay Sediment

Site 1a (Specimen MJ15/16) is a kaolinitic band at the top of the debris-flow sediments, very near their contact with the overlying, false-bedded, fluvial sediments. It is a chalky white to light-grey rock, consisting largely of kaolinite and quartz, with some smectite. Some surfaces are stained yellow-brown. It crumbles and reveals no tendency to slake in water or to become plastic. It is the water-lain, kaolinitic top of one of the debris-flows.

In thin section this rock consists of a very few shard-like quartz grains and flakey kaolinite 0.05-0.20 mm in size, set in a very fine-grained groundmass of quartz and kaolinite (shown by XRD). The whole is cut by open, arcuate desiccation cracks. Patches of the groundmass have been clouded with ultrafine kaolinite which has otherwise caused no fabric change. The edges of the ultrafine kaolinite are diffuse. The two kaolinite phases, the fine-grained, low birefringent kaolinite and the similar kaolinite which has been clouded, were analysed by microprobe. There are 11 analyses of the unclouded kaolinite (Appendix 1, Table 1A/23, Analyses 15.2-15.12) and 12 analyses of the clouded kaolinite (Appendix 1, Table 1A/24,

Figure 2

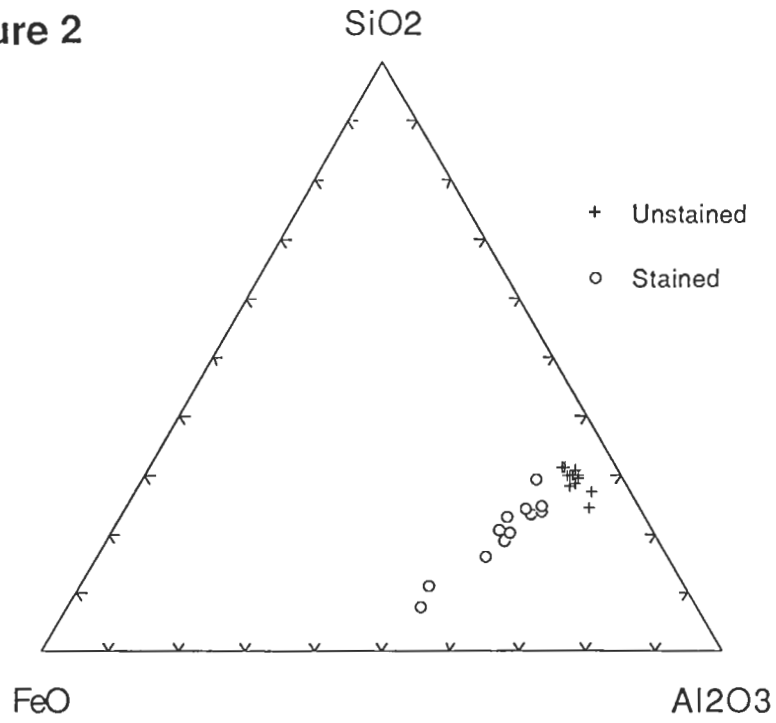


Figure 2. Segment of Si-Fe-Al ternary plot for stained and unstained kaolinites from the debris-flow sediment Specimen MJ5. Bottom left apex at SiO₂ 50%: FeO 10%: Al₂O₃ 40%. Tick marks at 1%.

Figure 3

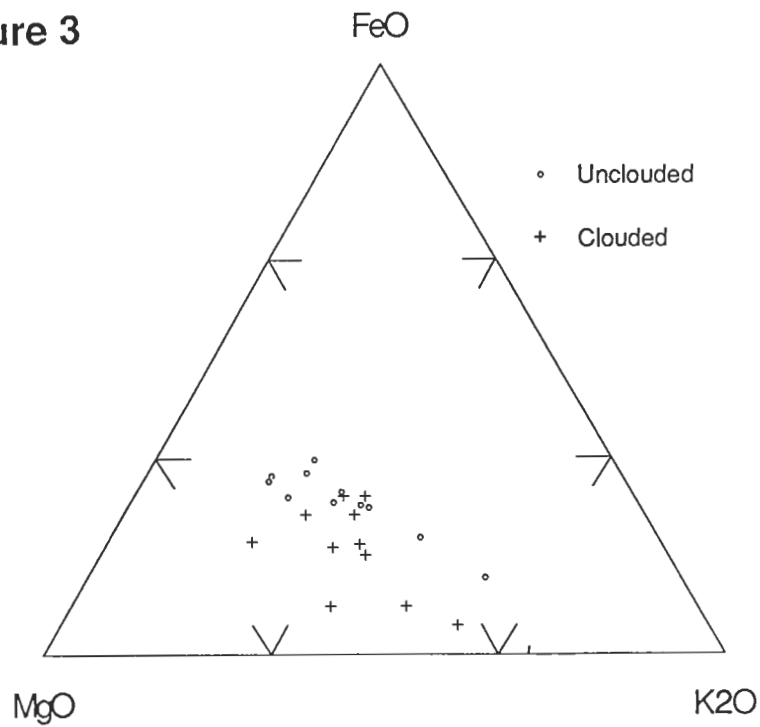


Figure 3. Segment of Fe-Mg-K ternary plot for clouded and unclouded kaolinites from clay sediment Specimen MJ15/16. Bottom left apex at FeO 30%: MgO 60%: K₂O 10%. Tick marks at 10%.

Analyses 15.15-15.26). The means of the structural formulae of these two kaolinite types are presented in Table 8. There is no significant difference between these two kaolinite types (95% confidence limits) in all elements except for Fe which is slightly poorer in the clouded kaolinite. Though the differences are not significant at the 95% confidence limits, the t values are slightly high for Mg and K, the clouded kaolinites being very slightly richer in both. The ternary diagram Fe-Mg-K (Figure 3) illustrates this.

TABLE 8

KAOLINITES OF MJ15

| | <i>Fine-grained</i> | <i>S.Dev</i> | <i>Clouded</i> | <i>S.Dev</i> | <i>t</i> |
|------|---------------------|--------------|----------------|--------------|----------|
| Si | 4.311 | 0.027 | 4.306 | 0.027 | -0.424 |
| Al | 3.333 | 0.030 | 3.335 | 0.044 | 0.121 |
| Ti | 0.017 | 0.004 | 0.019 | 0.006 | 0.890 |
| Fe+2 | 0.082 | 0.004 | 0.076 | 0.004 | -3.434* |
| Mn | 0.000 | - | 0.000 | - | - |
| Mg | 0.165 | 0.008 | 0.169 | 0.009 | 1.073 |
| ΣOct | 3.597 | - | 3.600 | - | - |
| Ca | 0.058 | 0.002 | 0.057 | 0.004 | -0.715 |
| Na | 0.013 | 0.003 | 0.014 | 0.002 | 0.905 |
| K | 0.064 | 0.018 | 0.074 | 0.019 | 1.235 |
| ΣLC | 0.135 | - | 0.145 | - | - |
| n | 11 | - | 12 | - | v=21 |

Critical value of t at 95% confidence limits is ± 2.08

It is concluded that this kaolinite phase, which shows a little more Si than ideal, is a fine-grained, waterlain kaolinite, slightly mixed with ultra fine-grained quartz. Weathering has locally recrystallised the kaolinite and a small fraction of Fe has been removed and redeposited. An SEM examination of this kaolinite phase (Specimen MJ15) reveals a compact, flakey to earthy fabric with poorly-formed crystals of no more than 1 μm . No elongate structures (halloysite) were seen.

The coarse-grained micaceous kaolinites, which occur in the fine-grained matrix as patches and distorted stacks with first order white to pale yellow birefringence, were briefly examined by microprobe. Two were analysed in the clear area (Appendix 1, Table 1A/25, Analyses 15.13; 15.14) and two were analysed in the cloudy area (Appendix 1, Table 1A/25, Analyses 15.27; 15.28). The structural formulae of these are shown in Table 9. They have been plotted for comparison with the clouded and unclouded fine-grained kaolinites on the Ti-Fe-K-Mg diagram (Appendix 2, Figure 2A/2). It is clear that, though the clouded and unclouded fine-grained kaolinites form a coherent group, the coarse-grained kaolinites are completely separate and are Ti free. It is concluded that the coarse grained kaolinite is not a product of recrystallisation of the matrix but represents a completely separate phase which is probably detrital and very likely derived from material of a similar fabric to the kaolinised granite saprolite.

TABLE 9

COARSE-GRAINED KAOLINITES OF MJ15

| No | From Clear Area | | Mean | From Clouded Area | | Mean |
|----|-----------------|-------|-------|-------------------|-------|-------|
| | 15.13 | 15.14 | - | 15.27 | 15.28 | - |
| Si | 4.095 | 4.077 | 4.086 | 4.164 | 3.999 | 4.082 |
| Al | 3.790 | 3.783 | 3.787 | 3.684 | 3.957 | 3.821 |
| Ti | 0.000 | 0.000 | 0.000 | 0.000 | 0.000 | 0.000 |
| Fe | 0.045 | 0.047 | 0.046 | 0.070 | 0.037 | 0.054 |
| Mg | 0.046 | 0.056 | 0.051 | 0.049 | 0.016 | 0.033 |
| Ca | 0.019 | 0.032 | 0.026 | 0.016 | 0.009 | 0.013 |
| Na | 0.003 | 0.004 | 0.004 | 0.000 | 0.003 | 0.002 |
| K | 0.025 | 0.072 | 0.049 | 0.018 | 0.009 | 0.014 |

COMPARISONS OF MINERAL PHASES

The Primary Mineralogy of Specimen MJ8 and Specimen MJ10 (Pink Granite)

The three feldspar phases of Specimen MJ8 and Specimen MJ10 were compared to determine the extent of variation between samples.

The K-feldspars are essentially identical in composition except perhaps for Al which is statistically slightly more abundant in Specimen MJ8. These feldspars are compared in Table 10 (see also Appendix 1, Tables 1A/6 and 1A/4).

TABLE 10

COMPARISON OF THE K-FELDSPAR PHASES
OF MJ8 and MJ10

| | MJ8 | | Mean | MJ10 | | t |
|------|-------|-------|-------|-------|--------|---|
| | Mean | S.Dev | | S.Dev | | |
| Si | 2.975 | 0.009 | 2.979 | 0.006 | 0.675 | |
| Al | 1.024 | 0.001 | 1.019 | 0.006 | 3.488* | |
| Fe+3 | 0.013 | 0.018 | 0.006 | 0.004 | -0.899 | |
| Mg | 0.002 | 0.003 | 0.001 | 0.002 | -0.506 | |
| Ca | 0.000 | 0.000 | 0.000 | 0.000 | - | |
| Na | 0.043 | 0.016 | 0.045 | 0.014 | 0.157 | |
| K | 0.959 | 0.010 | 0.970 | 0.010 | 1.245 | |
| Ti | 0.000 | 0.000 | 0.000 | 0.000 | - | |
| Mn | 0.000 | 0.000 | 0.000 | 0.000 | - | |
| Ab | 4.3 | 1.6 | 4.5 | 1.4 | 0.157 | |
| An | 0.0 | 0.0 | 0.0 | 0.0 | - | |
| Or | 95.8 | 1.6 | 95.5 | 1.4 | -0.235 | |
| n | 2 | | 8 | | | |

Critical Value for t is ± 2.31

The plagioclases, however, (Appendix 1, Tables 1A/3 and 1A/5) show significant differences. The plagioclase of Specimen MJ8 is significantly depleted in Ca and K and enriched in Na compared to Specimen MJ10. This is illustrated by Table 11 and Figure 4. These differences may reflect a state of partial alteration which was noted in the petrographic study and should be worthy of TEM investigation, however one plagioclase analysis of Specimen MJ10 (analysis 10.21) overlaps with the Specimen MJ8 data. The differences could be also, in part, due to scarce data.

TABLE 11
COMPARISON OF THE SEPARATE PLAGIOCLASE PHASE
OF MJ8 AND MJ10

| | MJ8 | | MJ10 | | <i>t</i> |
|------|-------------|---------------|-------------|---------------|----------|
| | <i>Mean</i> | <i>S. Dev</i> | <i>Mean</i> | <i>S. Dev</i> | |
| Si | 2.959 | 0.002 | 2.956 | 0.010 | -0.471 |
| Al | 1.047 | 0.004 | 1.053 | 0.008 | 1.139 |
| Fe+3 | 0.001 | 0.002 | 0.000 | 0.000 | -1.369 |
| Mg | 0.001 | 0.002 | 0.000 | 0.000 | -1.369 |
| Ca | 0.018 | 0.003 | 0.033 | 0.007 | 3.289* |
| Na | 0.972 | 0.009 | 0.936 | 0.015 | -3.586* |
| K | 0.007 | 0.003 | 0.014 | 0.004 | 2.539* |
| Ti | 0.000 | 0.000 | 0.000 | 0.000 | - |
| Mn | 0.001 | 0.001 | 0.000 | 0.000 | - |
| Ab | 97.5 | 0.4 | 95.3 | 1.0 | -3.389* |
| An | 1.8 | 0.3 | 3.3 | 0.7 | 3.289* |
| Or | 0.7 | 0.3 | 1.7 | 1.0 | 1.558 |
| n | 3 | | 9 | | |

Critical value for *t* is ± 2.23

The plagioclase phase of the perthite was only briefly examined (2 analyses for Specimen MJ8 and 1 for Specimen MJ10). All are albite and the perthite plagioclase phase is less calcic than the separate co-existing plagioclase phase, as would be expected (Appendix 1, Tables 1A/26 and 1A/7). The perthite plagioclase of Specimen MJ8 contains appreciable potassium but the number of analyses is too low for much significance to be placed upon it.

The chlorites and chloritised biotites of Specimen MJ8 were extensively analysed by microprobe. Those with less than 0.5% K₂O were classed as chlorites (Appendix 1, Table 1A/1) and their structural formulae were calculated accordingly. The high iron content and high Fe/(Fe+Mg) ratio defines this unoxidised chlorite as a Brinsvigite (Hey, 1954). The manganese content is unusually high (1.23%). The sum of the octahedral ions is within 6% of the ideal 12.

The majority of the microprobed chlorites contained a significant quantity of K₂O (>0.5-2.57) due to admixture with biotite (Appendix 1, Table 1A/2). Again the manganese content is unusually high and also Si, which is consistent with admixture with biotite. Each analysis was normalised to a 100% total and each oxide was regressed against K₂O to determine its intercept where K₂O is zero. All elements but Mg gave

Figure 4

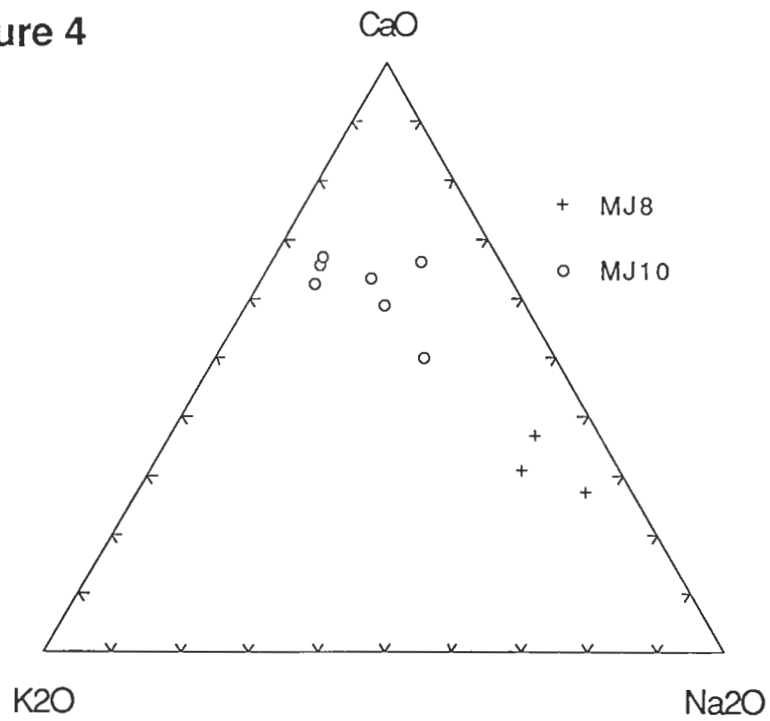


Figure 4. Segment of Ca-K-Na ternary plot for plagioclases of pink granite Specimens MJ8 and MJ10. Bottom left apex at CaO 0%: K₂O 10%: Na₂O 90%. Tick marks at 1%.

Figure 5

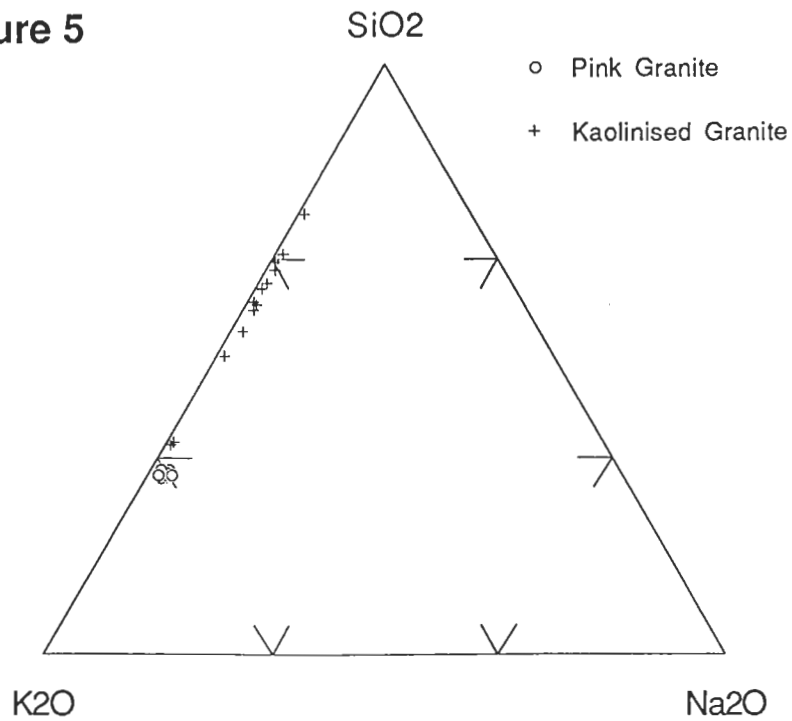


Figure 5. Segment of Si-K-Na ternary plot for K-feldspars of pink granite and kaolinised granite. Bottom left apex at SiO₂ 70%: K₂O 30%: Na₂O 0%. Tick marks at 10%.

good regressions. As would be expected Al and Fe both show a negative correlation with K and Si a positive correlation as the chlorite-biotite mixtures tend towards biotite. An hypothetical pure chlorite component was determined from this and its structural formula calculated (Table 12). This was further investigated using J.L. Walsh's chlorite program. Due to the uncertainty of the MgO value, two runs were carried out, using the limiting values of 4.59% and 5.50% MgO.

TABLE 12
MJ8 AND 10
HYPOTHETICAL PURE CHLORITE

| | |
|----------------|--------|
| Si | 5.911 |
| Al | 2.089 |
| <hr/> | |
| Σ Tet | 8.000 |
| <hr/> | |
| Al | 3.103 |
| Ti | 0.006 |
| Fe+2 | 6.753 |
| Mn | 0.199 |
| Mg | 1.353 |
| <hr/> | |
| Sum Oct | 11.414 |
| <hr/> | |
| Ca | 0.059 |
| Na | 0.027 |
| K | 0.000 |
| <hr/> | |
| Σ Large | 0.086 |

The results gave limiting temperatures for chlorite at 183.5°C and 193.5°C respectively and the chlorites are shown to be strongly reduced. It is possible that the chlorite model underestimates the temperatures by about 40°C over this temperature range, so the temperature of chlorite formation could be as high as 220°C. Intuitively it is thought that these temperatures reflect the cooling history of the granite rather than any hydrothermal system. Further sampling of chloritic granite would have to be done at various distances from the tin mine to prove this but exposure precluded such an investigation.

Microprobe analyses of the muscovites of Specimen MJ10 are given in Appendix 1, Table 1A/8. These conform quite well to the muscovite formula and are quite consistent in their Si and Al contents but show considerable variation in their Fe (5.27-0.81%) and to a lesser extent in their K (10.71-5.75%) contents. The variation in birefringence seems linked to their iron content. It is possible that these muscovites are showing incipient alteration prior to kaolinisation.

The K-feldspars of Kaolinised Granites: Specimens MJ7 and 9

The only primary minerals that survive into the kaolinitic granite and the 'greisen funnel' are quartz and K-feldspar. No significant changes were expected in quartz so it was not studied further. A number of K-feldspars were analysed by microprobe in Specimen MJ7 (12) and Specimen MJ9 (5) and their analyses

are presented in Appendix 1, Tables 1A/11 and 1A/14. One of the twelve K-feldspar analyses of Specimen MJ7 has an anomalously low total and at least four of the five K-feldspars of Specimen MJ9 are significantly low in total. The silica contents are unusually high and potassium is low. If the average K-feldspars of the pink granites of Specimen MJ8 and Specimen MJ10 are compared statistically to the K-feldspars of the kaolinised granites of Specimen MJ7 and Specimen MJ9 (Table 13), Si is found to be enriched and Na and K are depleted in the feldspars of the kaolinised granites. In Specimen MJ7, Fe is depleted as well. The K-feldspars of the pink granites (Specimen MJ8 and Specimen MJ10) show a constant Si/K ratio with a variable Na content (see Figure 5) but the K-feldspars of the kaolinised granites (Specimen MJ7 and Specimen MJ9) do not. They are more Si rich and have a variable Si/K ratio, those of Specimen MJ7 being more Na rich than those of Specimen MJ9. Three from Specimen MJ9 fall on the extension of the K-feldspar trend and this is in part confirmed by their overall chemistry. This suggests an alteration process or simplification of their chemistry and may indicate very fine scale non-disruptive partial kaolinisation. Apart from undulose extinction, this was not apparent in the thin section study. Clearly an XRD and a TEM study are required here.

TABLE 13

TWO-WAY COMPARISON OF AN AVERAGE
MJ8 - MJ10 K-FELDSPAR WITH
THE K- FELDSPARS OF MJ7 AND 9

| | <i>t</i> | MJ7 | | MJ8-10 | | MJ9 | | <i>t</i> |
|------------------|----------|-------------|---------------|-------------|---------------|-------------|--------------|----------|
| | | <i>Mean</i> | <i>S. Dev</i> | <i>Mean</i> | <i>S. Dev</i> | <i>Mean</i> | <i>S.Dev</i> | |
| Si | 18.74* | 3.092 | 0.017 | 2.977 | 0.008 | 3.036 | 0.030 | 5.42* |
| Al | 9.74* | 1.042 | 0.005 | 1.022 | 0.004 | 1.017 | 0.019 | -0.74 |
| Fe ⁺³ | -2.65 | 0.001 | 0.002 | 0.010 | 0.011 | 0.000 | 0.000 | -1.99 |
| Mg | -2.20* | 0.000 | 0.000 | 0.002 | 0.003 | 0.000 | 0.000 | -1.39 |
| Na | -3.42* | 0.026 | 0.008 | 0.044 | 0.015 | 0.019 | 0.001 | -3.47* |
| K | -20.32* | 0.476 | 0.072 | 0.965 | 0.01 | 0.786 | 0.171 | -2.98* |
| n | | 12 | | 10 | | 5 | | |

Critical t value is ± 2.09 Critical t value is ± 2.16

Coarse-grained Kaolinites and Micas of the Granite and Kaolinised Granite

The coarse-grained kaolinites and muscovites of the kaolinised granites (Specimen MJ6,7,9, and 11) and a pink granite (Specimen MJ10) are compared. Petrographic evidence (Specimen MJ6, 7,9 and 11) clearly indicates an alteration process of muscovite to kaolinite. In some, thin layers of extremely low birefringent kaolinite are found interleaved with highly birefringent muscovite. The junction between the two phases is sharp. In other instances, coarse-grained, rather micaceous kaolinite occurs as flakes within a fine-grained kaolinite which appears to have been derived by alteration of a plagioclase. The coarse-grained kaolinite mimics the muscovite flakes, often found in the unaltered plagioclase. The birefringence of the coarse-grained kaolinite tends to vary from grey to yellow. In places it occurs as distorted stacks and books but, unlike the interleaved muscovite and kaolinite, only one phase is visible under the petrographic microscope.

Microprobe analyses of these phases are given in Appendix 1, Tables 1A/20, 1A/18 and 1A/8 (muscovite), Table 1A/17 (kaolinite) and in Tables 1A/13 and 1A/10 (anomalously birefringent kaolinite). The muscovites are variable in K_2O (10.71-3.79%) and in FeO (5.27-0.91). The kaolinite and anomalously birefringent kaolinite are similarly variable (K_2O 5.85-0.22 and FeO 5.61-0.52). The birefringence of the kaolinite is clearly linked to the FeO content and not to K_2O (Appendix 1, Tables 1A/10, 1A/13).

The tetrahedron plots for Si-Al-Mg-Fe (Appendix 2, Figure 2A/3), Si-Al-K-Mg (Appendix 2, Figure 2A/4), Si-Al-K-Na (Appendix 2, Figure 2A/5) and Si-Al-K-Fe (Appendix 2, Figure 2A/6) clearly show a trend from the muscovites of Specimen MJ9 and Specimen MJ10 to the kaolinites of Specimen MJ9. Some of the moderately birefringent kaolinites have intermediate compositions, some are very like the kaolinites in composition and some muscovites of Specimen MJ6 also have an intermediate composition. In all instances a constant Si/Al ratio of nearly 1:1 is maintained. Figure 2A/6 of Appendix 2 is particularly interesting as it shows a separate trend towards iron among the potassium-poor birefringent coarse-grained kaolinites, illustrating the correlation of iron content with birefringence.

Kaolinites of the Debris-flow Sediments

The relevant samples are Specimen MJ13, a relatively coarse-grained quartz-bearing kaolinitic sediment, from the base of the debris-flow sediments, and Specimen MJ15, a sample of the kaolinitic layer marking the top of the debris-flow sediments. The coarse-grained kaolinite of Specimen MJ13 covers a wide variety from low birefringent (dark grey: Appendix 1, Table 1A/27, analyses 13.61-77), through moderate birefringence (yellow-white: Appendix 1, Table 1A/28, Analyses 13.67-69). There are also a number of muscovite flakes (blue and red birefringence: Appendix 1, Table 1A/29, analyses 13.71-13.74). There appears to be a series of compositions from kaolinite to muscovite.

There are two kaolinite types in Specimen MJ15, a very fine-grained kaolinite, some of which is clouded (Appendix 1, Tables 1A/23 and 1A/24, Analyses 15.2-15.12, 15.15-15.26), and a flakey, coarser-grained kaolinite, which shows a variety of birefringence similar to the coarse-grained kaolinite of Specimen MJ13.

Chemically the muscovite of Specimen MJ13, the moderately birefringent kaolinites of Specimen MJ13 and Specimen MJ15 and the kaolinites of Specimen MJ13 form a series. The moderately birefringent kaolinites of Specimen MJ15 being chemically very alike to the low birefringent kaolinites of Specimen MJ13. The fine-grained kaolinites of Specimen MJ15 include a clouded phase (Appendix 1, Table 1A/24) and an unclouded phase (Appendix 1, Table 1A/23). These two fine-grained phases have already been shown to form a coherent, titaniferous group (see under Specimen MJ15/16), which is markedly different from the coarse-grained kaolinites which are Ti-free. Compared to this group, the coarse-grained kaolinites are enriched in Al and depleted in Si, Ti, Mg, Ca and Na. The more birefringent kaolinites are enriched in Fe, Mn and K, showing the transition from muscovite to kaolinite. The difference between the two

kaolinite types is well-illustrated in Appendix 2, Figures 2A/7-10.

The coarse-grained kaolinites show an almost complete path from muscovite to kaolinite on the Si-Al-K-Na and the Si-Al-K-Fe plots (Appendix 2, Figure 2A/11 and 2A/7) at a constant Si/Al ratio. The fine-grained kaolinite shows a shorter, separate though parallel trend at a higher Si/Al ratio. The Si-Al-K-Mg plot (Appendix 2, Figure 2A/8) is similar but the fine-grained kaolinites show a close grouping and are separate from the coarser-grained kaolinite to muscovite trend. The iron enrichment of the coarse-grained kaolinite is very apparent on the Si-Al-Mg-Fe plot (Appendix 2, Figure 2A/9) compared to the tight grouping of the more Mg-rich fine-grained kaolinite. The two groups form separate clouds on the Fe-Mg-K-Na plot (Appendix 2, Figure 2A/10).

If the corresponding tetrahedron plots are overlaid (Appendix 2, Figures 2A/7-10, Figure 2A/12 and Figures 2A/3-6) there is a very strong similarity between the coarse-grained kaolinite and muscovite of the debris-flow sediments and those of the underlying kaolinised granite. This may be used to confirm that the sediments were locally derived from a similar weathered granite source rock.

Kaolinites after Plagioclase.

All the kaolinites in Specimens MJ6-7, Specimen MJ9 and Specimen MJ11 that appear to be pseudomorphing plagioclase have been plotted for comparison. They form a relatively tight group, though there are minor differences. The kaolinite after the plagioclase of the perthite is essentially indistinguishable from the rest. There seems to be a trend towards alkali (K, Na) enrichment for those higher in the profile or further from the 'centre of hydrothermal activity', depending upon one's preference. The plots in Appendix 2, Figures 2A/13-17 refer.

Coarse- and Fine-grained Kaolinites

Here the kaolinites derived from plagioclase and the relatively coarse-grained kaolinites and kaolinised micas are compared for samples MJ6-7, MJ9-11. Plots in Appendix 2, Figures 2A/18-22 refer. The kaolinites derived from plagioclase form a tight grouping while the micaceous kaolinites do not. Where the coarse-grained kaolinites are poor in K and Fe, the two populations are relatively similar in composition but may still be distinguished. The kaolinite that pseudomorphs plagioclase tends to be poorer in K and richer in Al and Mg compared to their micaceous counterparts. The Fe-Mg-K-Na plot is particularly illustrative. There is a certain amount of overlap so it is very probable that application of Discriminant Analysis could improve the separation.

A TEM EXAMINATION OF COMPONENTS OF SPECIMEN MJ6

Specimen MJ6 was chosen for detailed TEM study as it lies close to the centre of the 'greisen funnel' and thus is most likely to show features which are unique to hydrothermal alteration, if such was the case at the Trial Hill Tin Mine. The five digit photo numbers refer to negative numbers lodged with the Centre for Australian Regolith Studies at the Australian National University in Canberra as evidence of this work.

Grid #3 Material:- K-feldspar with kaolinised perthite

Photos 31333-479

The K-feldspar, which appears to be unaltered, shows a smoothly curved contact with its intergrown, completely kaolinised perthite component (Plate 5A). The kaolinised component consists entirely of rolled tubes of halloysite of 0.08-0.16 μm cross section and 0.5 μm length. They show characteristic polygonal cross sections, though a few are oval. Most show hollow centres and wedge-shaped voids near the angles of the polygons (Plates 5A and B). The halloysite is readily damaged by the electron beam. Though the halloysite is mainly recognised on morphological grounds, ring diffraction patterns showed that it is 7- \AA halloysite. Recognisable diffraction patterns were obtained from the fresh K-feldspar on [310] and [200].

Grid #6 Material:- Mixed mica - moderate birefringence

Photos 31950-32005

There are two clay phases, rolled tubes of halloysite and a mica-like kaolinite. Though no muscovite diffraction patterns were obtained, some images of the sheet-like kaolinite show small layers and wisps of muscovite (10- \AA fringes) and the characteristic mottled diffraction contrast, typical of a mica. It seems the two phases, muscovite and slightly fanned kaolinite are intimately mixed. The relationship between the kaolinite and the halloysite phases is not all that clear, though there is some evidence that flakes of kaolinite, where they become detached from the main body of kaolinite, at the edge of a void, curl up and form rolled, irregular, polygonal halloysite tubes. In one photo there is evidence of a 14- \AA structure.

Grid #2 Material:- Kaolinised Plagioclase

Photos 32006-32030

The diffraction patterns show an halloysite ring pattern, oriented kaolinite and oriented muscovite. The images indicate that the kaolinite and muscovite phases are mixed and aligned but the quality of the photography was not good enough to see this interlamination in detail. Narrow, dark strips of apparent muscovite, showing mottled diffraction contrast, lie within and parallel to the oriented kaolinite. Some of the kaolinite occurs in vermiform stacks, with partings at 500-1500- \AA intervals. Halloysite occurs between the books and stacks of kaolinite.

PLATE 5

Partly kaolinised K-feldspar perthite.

A. A smooth contact between fresh K-feldspar (KF) and a spiral roll of halloysite (HA). Note the hollow core and polygonal structure of the spiral. Linear parts of the polygons show mottled diffraction contrast (MD). The spiral is set amidst some halloysite longitudinal sections. Photo 31409. Grid #3. Specimen MJ6.

B. Longitudinal sections of halloysite spirals (HA), showing hollow cores (C), together with a few small spiral cross sections (HS). Photo 31411. Grid #3. Specimen MJ6.

Kaolinised Plagioclase

C. Sheets of kaolinite showing mottled diffraction contrast, passing into a polygonal halloysite spiral (HS). Linear parts of the polygonal spiral show mottled diffraction contrast (MD), due to relics of kaolinite in the halloysite. Photo 32021. Grid #2. Specimen MJ6.

Intergrown Clay and Separate Birefringent Muscovite

D. Muscovite showing patches of 10-Å fringes (A) as well as 20-Å fringes (B), indicate a component of the 2M1 polymorph. A lenticular parting (LN) cuts the crystal. Photo 32099. Grid#12. Specimen MJ6.

E. Largely kaolinite (KA), showing mottled diffraction contrast (MD) in places, with very thin, but persistent, layers of muscovite (MU) interleaved with it. Note curled-over edge of the kaolinite, due to distortion from electron beam damage. Photo 32045. Grid 12. Specimen MJ6.

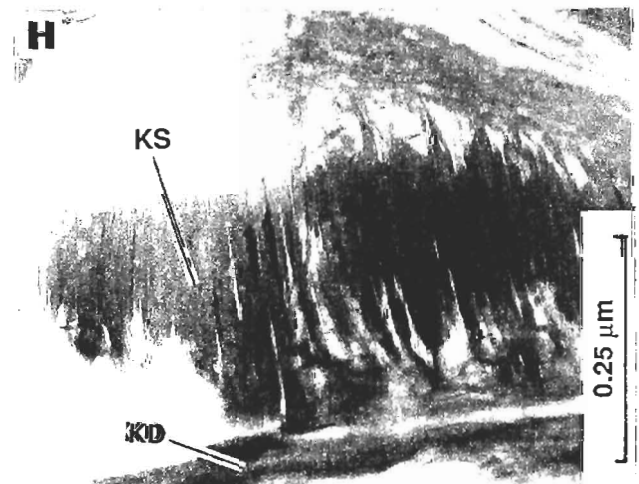
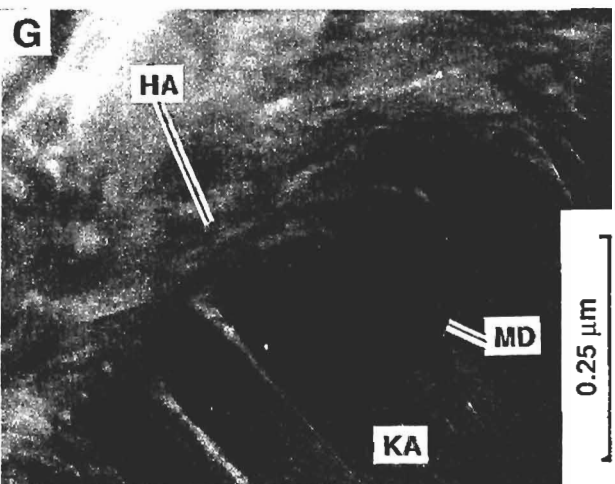
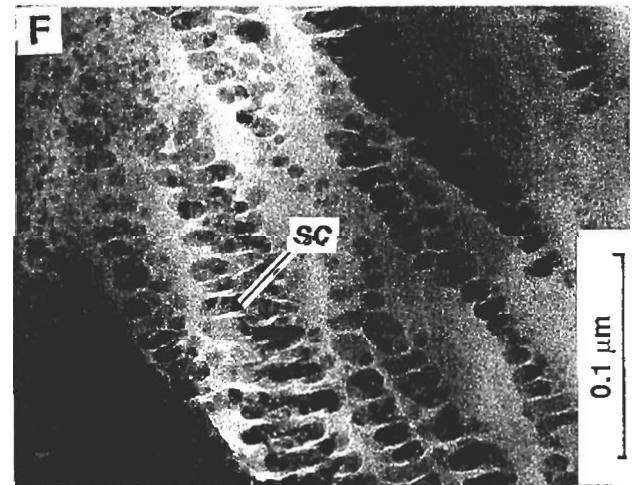
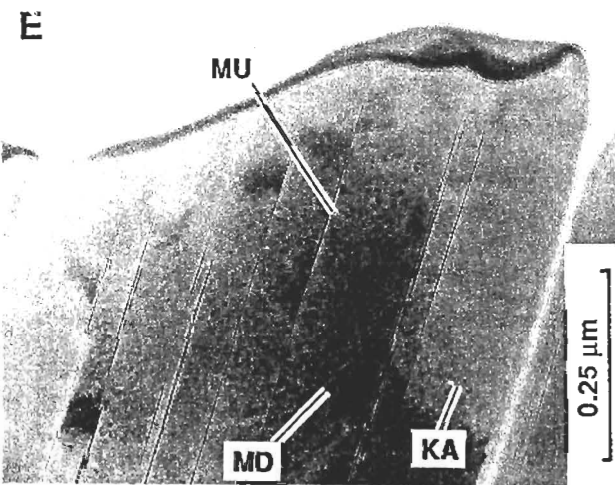
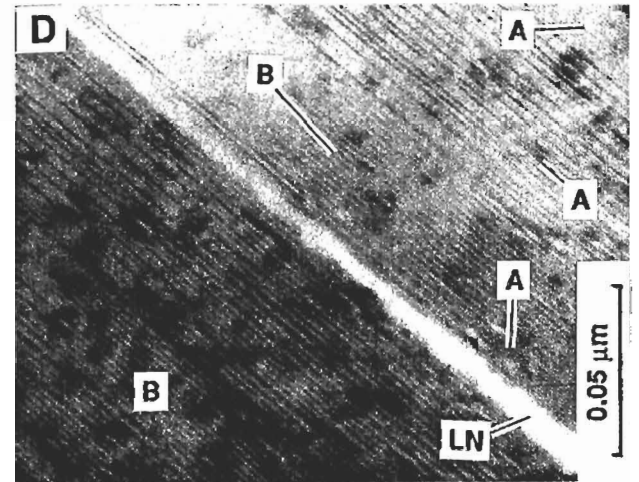
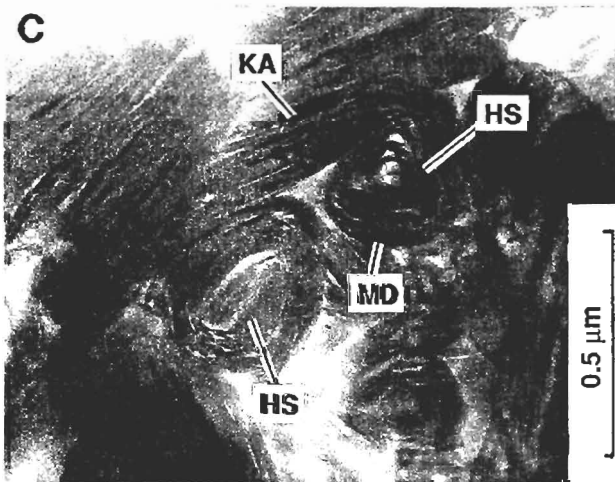
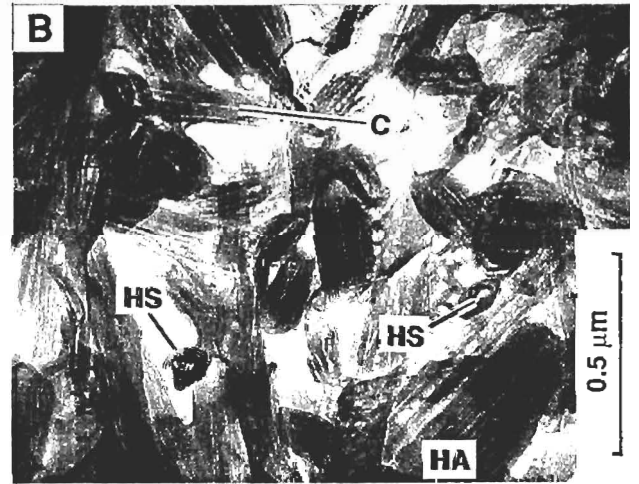
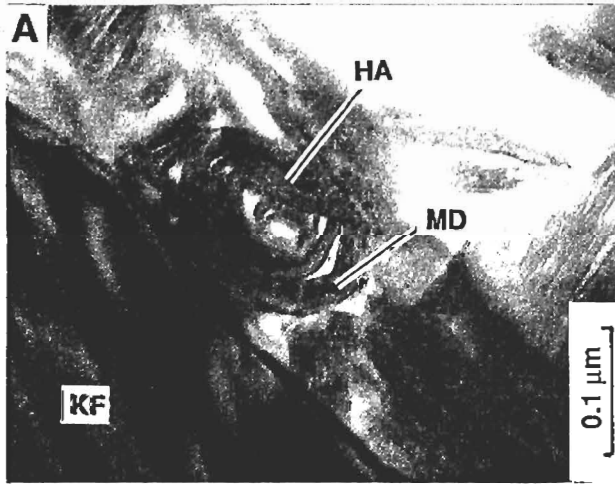
F. A blob-like phase (SC) with a 'cumulo-cirrus' fabric, occurs along the edges of voids in the phyllosilicate mass. This has not been identified. Photo 32067. Grid 12. Specimen MJ6.

Low Birefringent mixed kaolinite and mica

G. The end of a book of kaolinite (KA), showing some mottled diffraction contrast (MD). Here the kaolinite structure becomes wispy and changes to sheaved halloysite (HA). Photo 32109. Grid #8. Specimen MJ6.

Intergrown Separate Kaolinite and Muscovite

H. A kaolinite stack (KS), set in sheets of beam-damaged kaolinite (KD). Photo 32395. Grid #9. Specimen MJ6.



One particularly clear picture (Plate 5C) shows strips of kaolinite that have rolled into spirals of halloysite. The rolling mechanism is not by simple curving of the kaolinite crystal. Several sharp kinks occur along the crystal at 1000-2000 Å intervals. This seems to be due to alteration of the kaolinite structure to halloysite, presumably by hydration, that causes the crystal to kink and curl at that point. As the alteration progresses, small relics of kaolinite are left behind, within the halloysite. These contribute rigidity and therefore linearity to the structure. Thus the most common forms of the rolled halloysite are irregular pentagons and hexagons and less-common forms are those that approximate quadrilaterals and triangles. Wedge-shaped gaps are common at or near the points of minimum radius. The whole much resembles a rolled newspaper. The fabrics indicate a progression from platy kaolinite to halloysite tubes. This has also been seen in the SEM study, where kaolinite platelets have halloysite tubes attached and partly fused with their surfaces.

Grid # 12 Material:- Intergrown separate kaolinite and highly birefringent muscovite

Photos 32031-32105

The diffraction patterns confirm kaolinite and muscovite. There are two main morphologies here, a layer-silicate, consisting of muscovite and kaolinite, and tubular halloysite. The halloysite shows polygonal cross-sections with a range in size from 500-3500 Å across. Its relationship to the muscovite and aligned kaolinite is rather uncertain but, in a few instances, it was seen to be at a very oblique angle to the layer-silicate structures and occurs at the ends of books of layer-silicate.

The layer-silicate phase consists of muscovite, showing mottled diffraction contrast and 10-Å fringes, which passes into a syntactic kaolinite phase. Some muscovites show 10/20-Å fringes (Plate 5D) and a slight kinking and waviness of the intermediate fringe occurs. Lenticular partings at intervals of 1100-2100 Å are common. Though, in general, the mica phase occupies large zones, in places the mica and kaolinite are intimately mixed (Plate 5E). The structure has been locally disrupted, where alteration of muscovite to clay has occurred. In places the alteration of muscovite to kaolinite may be seen at an advanced stage. Long strips of muscovite, showing 10-Å fringes, deeply penetrate the kaolinite and, in places along their length, one layer of the muscovite has locally collapsed to a 7-Å kaolinite structure. Lensoid voids, 80 Å wide and 1000 Å long, separate the structure at 600-Å intervals in an *en echelon* pattern.

Parts show muscovite, with a patchy appearance, altered syntactically to kaolinite. The diffraction pattern indicates oriented kaolinite and muscovite which is fanned. In places the layer-silicate structure has split open and tubes of halloysite, 2000 Å in diameter, wedges the layer-silicate apart. There is some evidence that the halloysite has developed by rolling up of kaolinite. Other parts show relict muscovite in kaolinite (which only shows traces of fringes). The kaolinite is particularly prone to electron beam damage.

A dot-like or blob-like phase also occurs (Plate 5F). In places this phase forms chains around the edges of voids and, where much of it occurs, it forms patches and parallel chains and 'cumulo-cirrus' fabrics. Some of these blobs are internally striped. Its nature is unknown.

Grid #8 Material:- Low birefringent mixed kaolinite-mica

Photos 32106-321 78

The diffraction patterns indicate kaolinite with a very small muscovite content. The images show largely kaolinite (no significant fringes but readily damaged by the electron beam) with some relict muscovite with mottled diffraction contrast. The muscovite content is about 30% or less and fringes are at 11.5-12.9 Å. Halloysite is relatively rare and occurs either at the ends of the layer-silicate books, where the kaolinite structure becomes disordered and wispy (Plate 5G), or where it occurs as rolls in partings in the layer-silicate which occur at intervals of 300-400 Å. The dot- or blob-like material occurs near the edges of voids.

The chief difference between these kaolinite patches of low to moderate birefringence and those containing discrete muscovite, with a high birefringence, discretely intergrown with kaolinite, is a far lower proportion of muscovite and only rare halloysite occurs in the kaolinite of low birefringence.

Grid #9 Material:- Intergrown separate kaolinite and muscovite phases

Photos 32179-32411

The diffraction patterns confirm both kaolinite and muscovite. The muscovite forms extensive sheets with partings at 250-1500 Å and the mica shows 10/20-Å fringes. The kaolinite is largely aligned and consists of slightly bent crystals of kaolinite, showing mottled diffraction contrast, interleaved with a minor amount of muscovite (9.7 Å). Here relict muscovite comprises only about 5% of the whole. At low magnification the kaolinite is, in places, found forming stacks (Plate 5H).

Only minor halloysite occurs in voids and partings in the layer silicate, though angular or bent and curved crystals of kaolinite are not uncommon. The ends of sheets, in books and stacks of kaolinite, show a tendency to curl. The comparative lack of tubular halloysite is probably related to a comparative lack of void space and a lack of freedom for the kaolinite crystals to be able to curl.

GEOCHEMISTRY

Methods

Two samples of the pink granite, four of the kaolinised granite, three of the debris-flow sediment and one of the clay sediment overlying the debris-flow material were geochemically analysed. The major elements were determined by XRF analysis of fused glass beads by the method of Norrish and Hutton (1969) on a Siemens SR300. The trace elements were determined on pressed pellets bound with PVA on a Phillips PW1400 by the methods of Norrish and Chappell (1977). XRF Sn analyses were performed by Analabs in Perth. Ferrous iron was determined after dissolution of the sample in hot H₂SO₄ and HF followed by titration against 0.005N K₂Cr₂O₇ in boric acid, H₂SO₄ and H₃PO₄, with barium diphenylamine sulphonate as indicator. Water and carbon dioxide were determined gravimetrically by the methods of Riley (1958) and

Hughes and Hannaker (1978). Bulk densities were determined by weighing and water displacement after coating in paraffin wax. The analytical data were transformed to a weight per unit volume basis (major elements as mg/ml and trace elements as $\mu\text{g/ml}$). All elements which showed a significant correlation were graphed. The geochemistry is given on a mass proportion basis in Table 14 and on a mass per unit volume basis in Table 15.

Major Elements

The kaolinised granite and the debris-flow material show very close geochemical affinities, which confirms that the latter was derived locally from the former. The plot of Si against S.G. (Figure 6) shows a linear progression of decreasing Si and S.G. from the pink granites, through the kaolinised granite and debris-flow material to the clay. The Ti/V plot shows a similar trend with increases in both elements in going from granite, through kaolinised granite and debris-flow sediment, to clay. The reverse is true for Rb/K Ba/Pb and Pb/Rb, demonstrating the various stages of K-feldspar destruction. The K/Na plot clearly illustrates the early destruction of plagioclase relative to K-feldspars in the kaolinised granite followed by progressive destruction of K-feldspar. K-feldspar is absent in the debris-flow sediment and in the clay layer.

The debris-flow material tends to be richer in Al, Ti and H_2O^+ , similar in total iron, Mg, Ca, H_2O^- and Na but significantly poorer in K than the kaolinised granite. This seems to reflect intense weathering, destruction of K-feldspar and kaolinisation, which could have occurred either in the upper parts of the saprolite, prior to erosion and sedimentation, or in the debris-flow sediment since deposition. The former is preferred.

The pink granites are significantly richer in Si, Ca, Na, K and Fe, similar in Mg, Ti and Al but poorer in H_2O^- and H_2O^+ than the kaolinised granite. All these alterations are much as would be expected if the kaolinised granite was a direct weathering product of the pink granite. Very similar trends were observed by Banfield (1985) in the weathering of granites in the Cooma area.

The Trace Elements

The trace element geochemistry of the pink granite and the kaolinised granite are remarkably similar on a mass per unit volume basis. There has been the expected loss due to weathering of some Si and Fe as well as Ca, Na, K, Rb, Sr with corresponding gains in H^+ , Al, and V. Ti, Mn, Ba, Pb, Sn and Zr have remained relatively stable. Depletions in Rb and Sr match those of K and Ca. Large-scale hydrothermal alteration would have caused significant changes in some of these elements in passing from the pink granite to the 'hydrothermal' kaolinised granite. This has not occurred. The changes in geochemistry are considered to be consistent with weathering. The trace element geochemistry of the debris-flow sediments is remarkably similar to that of the kaolinised granite. Though the debris-flow sediments are slightly enriched in Zr, Sn, and V, and depleted in Ba, Sr, K, Rb and Pb, this is consistent with derivation of the sediment from the most intensely weathered top of the granite saprolite.

TABLE 14

Weight %

| Field No Lab. No | PINK GRANITE | | KAOLINISED GRANITE | | | | DEBRIS-FLOW | | | CLAY |
|-----------------------------------|--------------|---------------|--------------------|--------------|--------------|---------------|--------------|--------------|---------------|---------------|
| | MJ8 ROB22 | MJ10 ROB24 | MJ6 ROB20 | MJ7 ROB21 | MJ9 ROB23 | MJ11 ROB25 | MJ3 ROB17 | MJ5 ROB19 | MJ13 ROB27 | MJ15 ROB29 |
| SiO ₂ | 76.94 | 77.11 | 70.06 | 72.80 | 73.63 | 73.30 | 75.22 | 74.19 | 67.53 | 48.20 |
| TiO ₂ | 0.06 | 0.06 | 0.07 | 0.08 | 0.08 | 0.07 | 0.18 | 0.13 | 0.09 | 0.45 |
| Al ₂ O ₃ | 12.35 | 12.76 | 17.81 | 16.86 | 16.71 | 15.47 | 18.14 | 17.48 | 22.14 | 30.89 |
| t. Fe ₂ O ₃ | 1.14 | 0.65 | 0.63 | 0.47 | 0.48 | 0.75 | 0.34 | 0.43 | 0.75 | 1.73 |
| Fe ₂ O ₃ | 0.66 | 0.53 | 0.57 | 0.39 | 0.42 | 0.67 | 0.29 | 0.38 | 0.68 | 1.61 |
| FeO | 0.44 | 0.10 | 0.05 | 0.07 | 0.06 | 0.07 | 0.04 | 0.04 | 0.06 | 0.10 |
| MnO | 0.04 | 0.01 | 0.01 | 0.01 | 0.01 | 0.01 | 0.01 | 0.01 | 0.01 | 0.01 |
| MgO | 0.14 | 0.17 | 0.24 | 0.23 | 0.24 | 0.17 | 0.10 | 0.18 | 0.20 | 1.18 |
| CaO | 0.18 | 0.19 | 0.11 | 0.11 | 0.12 | 0.10 | 0.06 | 0.08 | 0.11 | 0.43 |
| Na ₂ O | 3.22 | 2.73 | 0.36 | 0.29 | 0.30 | 0.35 | 0.29 | 0.33 | 0.32 | 0.28 |
| K ₂ O | 4.91 | 5.05 | 4.43 | 2.58 | 2.30 | 5.18 | 0.12 | 0.15 | 0.33 | 0.17 |
| P ₂ O ₅ | 0.03 | 0.01 | 0.02 | 0.01 | 0.01 | 0.01 | 0.01 | 0.02 | 0.01 | 0.03 |
| S | 0.00 | 0.00 | 0.00 | 0.00 | 0.00 | 0.00 | 0.01 | 0.01 | 0.00 | 0.00 |
| H ₂ O ⁺ | 0.57 | 0.94 | 4.79 | 5.01 | 4.67 | 3.53 | 6.16 | 6.02 | 7.88 | 11.59 |
| H ₂ O ⁻ | 0.25 | 0.42 | 1.11 | 1.40 | 1.25 | 0.83 | 0.64 | 0.77 | 1.07 | 4.69 |
| CO ₂ | 0.02 | 0.02 | 0.06 | 0.03 | 0.03 | 0.15 | 0.01 | 0.01 | 0.15 | 0.29 |
| TOTAL | 99.81 | 100.10 | 99.69 | 99.87 | 99.83 | 99.91 | 101.27 | 99.80 | 100.58 | 99.92 |
| S.G. | 2.49 | 2.41 | 1.98 | 1.83 | 1.86 | 1.90 | 2.02 | 1.94 | 2.14 | 1.59 |

ppm

| | | | | | | | | | | |
|----------|-----|------|-----|-----|-----|------|-----|-----|------|------|
| Ba | 52 | 52 | 66 | 70 | 66 | 64 | 1 | 1 | 4 | 22 |
| Rb | 414 | 424 | 364 | 217 | 200 | 461 | 21 | 23 | 58 | 14 |
| Sr | 23 | 23 | 17 | 14 | 14 | 17 | 6 | 6 | 12 | 18 |
| Pb | 25 | 27 | 48 | 36 | 34 | 28 | 13 | 12 | 10 | 17 |
| Zr | 90 | 93 | 104 | 125 | 128 | 96 | 173 | 149 | 185 | 183 |
| Nb | 12 | 13 | 12 | 13 | 15 | 14 | 23 | 19 | 14 | 27 |
| Y | 68 | 69 | 66 | 71 | 77 | 43 | 53 | 43 | 99 | 51 |
| Ce | 61 | 57 | 75 | 26 | 15 | 46 | 26 | 17 | 69 | 53 |
| Sc | 0.5 | 0.5 | 0.5 | 0.5 | 0.5 | 0.5 | 0.5 | 0.5 | 0.5 | 0.5 |
| V | 1 | 1 | 4 | 3 | 3 | 4 | 7 | 10 | 3 | 20 |
| Cr | 0.5 | 0.5 | 2 | 1 | 2 | 0.5 | 2 | 3 | 0.5 | 35 |
| Ni | 0.5 | 2 | 0.5 | 0.5 | 0.5 | 0.5 | 1 | 1 | 0.5 | 38 |
| Sn | 15 | 15 | 20 | 20 | 25 | 45 | 55 | 65 | 50 | 40 |
| Cu | 0.5 | 5 | 5 | 8 | 8 | 9 | 21 | 22 | 6 | 19 |
| Zn | 28 | 33 | 26 | 37 | 36 | 35 | 27 | 30 | 31 | 39 |
| Field No | MJ8 | MJ10 | MJ6 | MJ7 | MJ9 | MJ11 | MJ3 | MJ5 | MJ13 | MJ15 |

TABLE 15

mg/ml

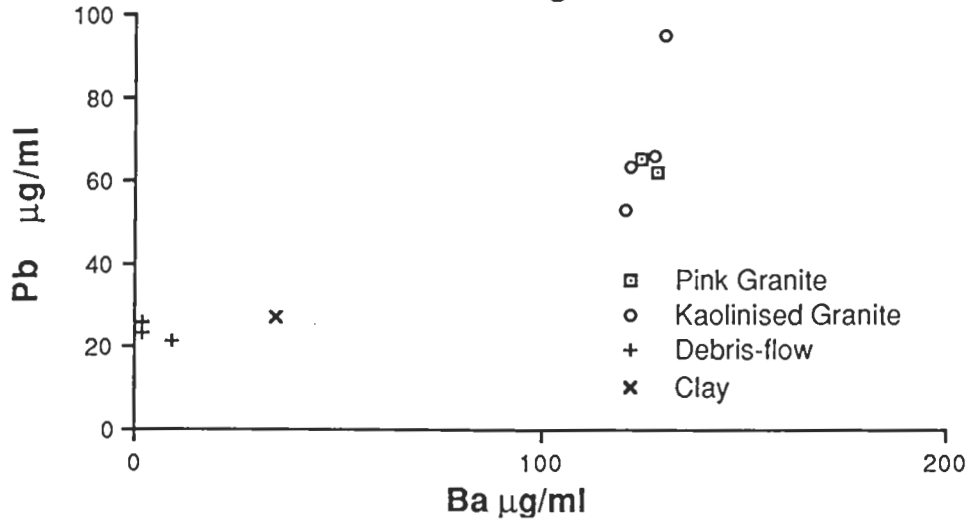
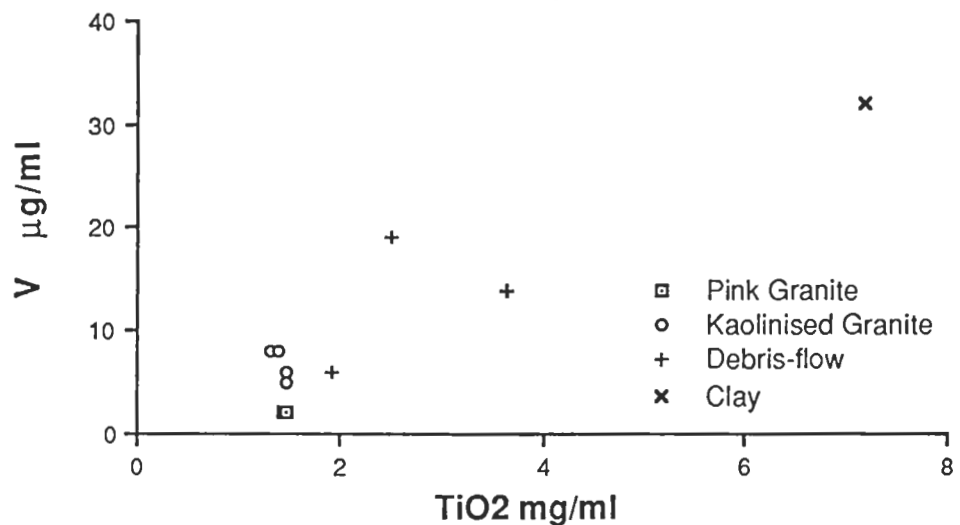
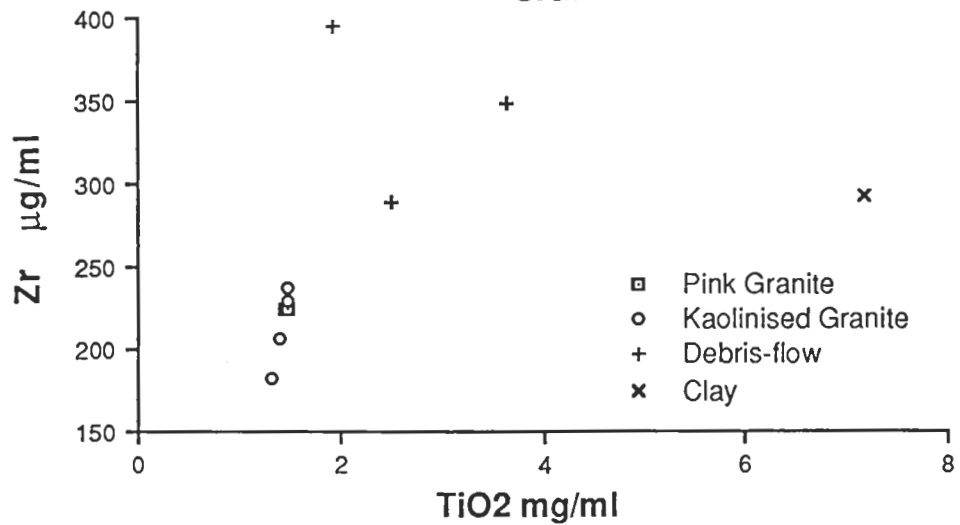
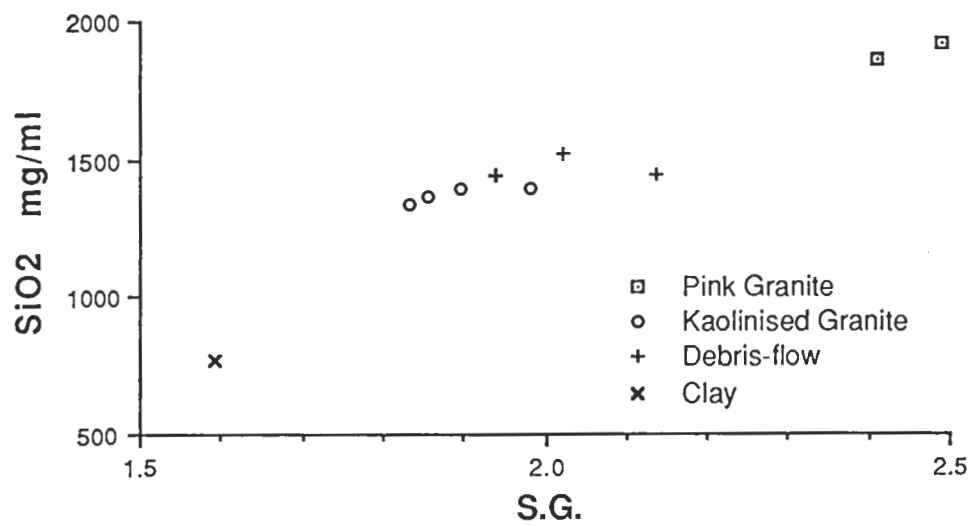
| Field No Lab. No | PINK GRANITE | | KAOLINISED GRANITE | | | | DEBRIS-FLOW | | | CLAY |
|-----------------------------------|--------------|---------------|--------------------|--------------|--------------|---------------|--------------|--------------|---------------|---------------|
| | MJ8 ROB22 | MJ10 ROB24 | MJ6 ROB20 | MJ7 ROB21 | MJ9 ROB23 | MJ11 ROB25 | MJ3 ROB17 | MJ5 ROB19 | MJ13 ROB27 | MJ15 ROB29 |
| SiO ₂ | 1915.81 | 1858.35 | 1389.29 | 1333.70 | 1365.84 | 1390.50 | 1519.44 | 1438.54 | 1443.12 | 768.31 |
| TiO ₂ | 1.49 | 1.45 | 1.39 | 1.47 | 1.48 | 1.33 | 3.64 | 2.52 | 1.92 | 7.17 |
| Al ₂ O ₃ | 307.52 | 307.52 | 353.17 | 308.88 | 309.97 | 293.47 | 366.43 | 338.94 | 473.13 | 492.39 |
| t. Fe ₂ O ₃ | 28.39 | 15.67 | 12.49 | 8.61 | 8.90 | 14.23 | 6.87 | 8.34 | 16.03 | 27.58 |
| Fe ₂ O ₃ | 16.43 | 12.77 | 11.30 | 7.14 | 7.79 | 12.71 | 5.86 | 7.37 | 14.53 | 25.66 |
| FeO | 10.96 | 2.41 | 0.99 | 1.28 | 1.11 | 1.33 | 0.81 | 0.78 | 1.28 | 1.59 |
| MnO | 1.00 | 0.24 | 0.20 | 0.18 | 0.19 | 0.19 | 0.20 | 0.19 | 0.21 | 0.16 |
| MgO | 3.49 | 4.10 | 4.76 | 4.21 | 4.45 | 3.22 | 2.02 | 3.49 | 4.27 | 18.81 |
| CaO | 4.48 | 4.58 | 2.18 | 2.02 | 2.23 | 1.90 | 1.21 | 1.55 | 2.35 | 6.85 |
| Na ₂ O | 80.18 | 65.79 | 7.14 | 5.31 | 5.57 | 6.64 | 5.86 | 6.40 | 6.84 | 4.46 |
| K ₂ O | 122.26 | 121.71 | 87.85 | 47.27 | 42.67 | 98.26 | 2.42 | 2.91 | 7.05 | 2.71 |
| P ₂ O ₅ | 0.75 | 0.24 | 0.40 | 0.18 | 0.19 | 0.19 | 0.20 | 0.39 | 0.21 | 0.48 |
| S | 0.00 | 0.00 | 0.00 | 0.00 | 0.00 | 0.00 | 0.20 | 0.19 | 0.00 | 0.00 |
| H ₂ O+ | 14.19 | 22.65 | 94.99 | 91.78 | 86.63 | 66.96 | 124.43 | 116.73 | 168.40 | 184.74 |
| H ₂ O- | 6.23 | 10.12 | 22.01 | 25.65 | 23.19 | 15.75 | 12.93 | 14.93 | 22.87 | 74.76 |
| CO ₂ | 0.50 | 0.48 | 1.19 | 0.55 | 0.56 | 2.85 | 0.20 | 0.19 | 3.21 | 4.62 |

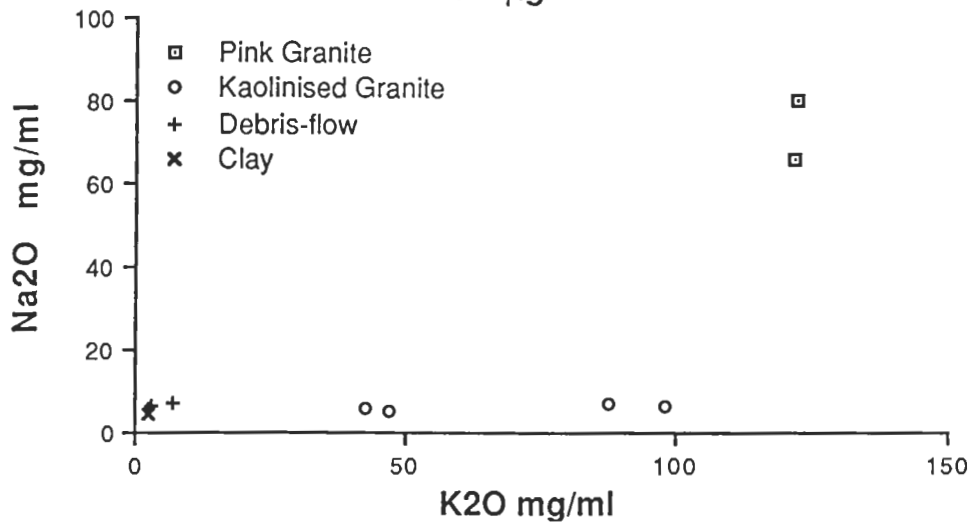
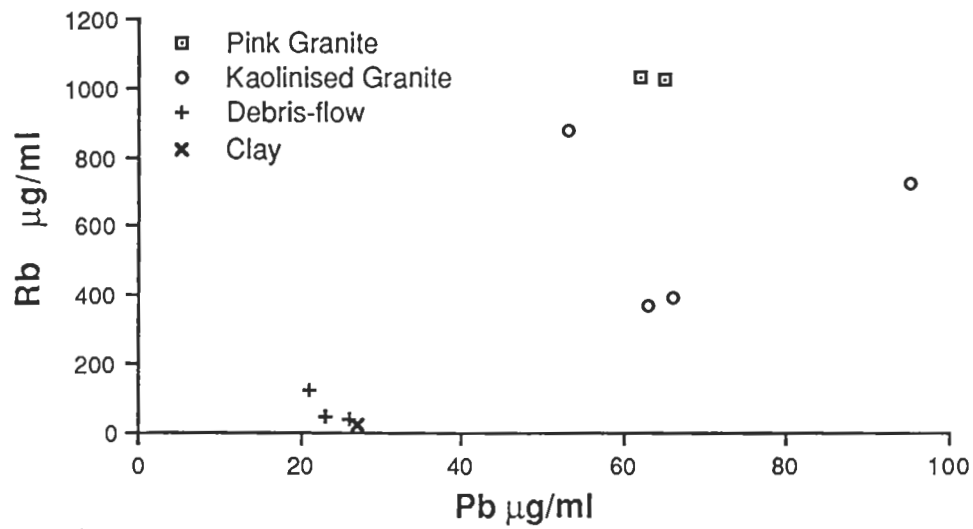
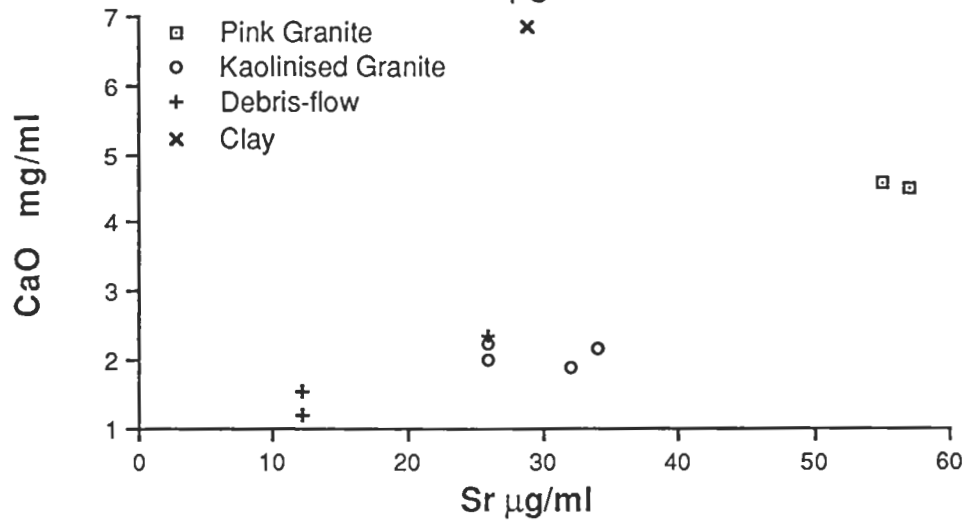
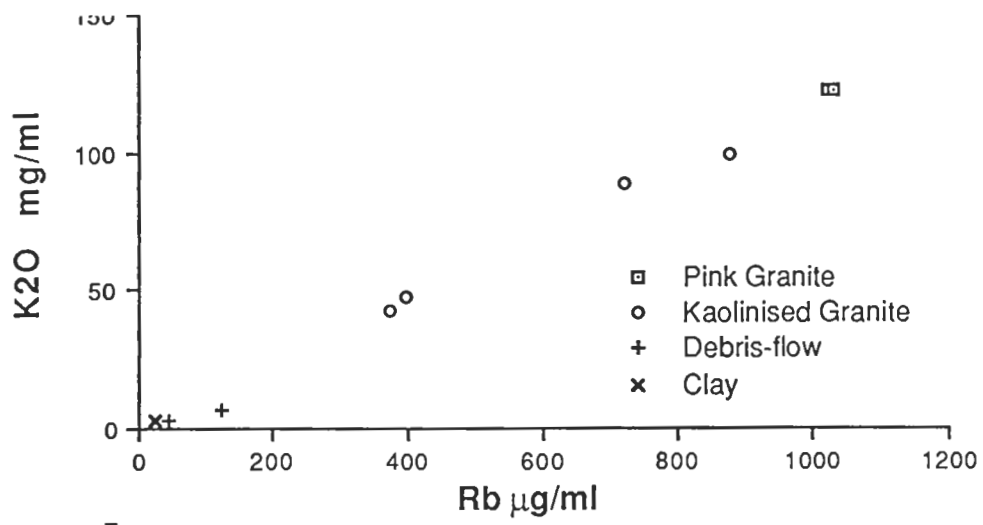
µg/ml

| | | | | | | | | | | |
|----------|------|------|-----|------|------|------|------|------|------|------|
| Ba | 129 | 125 | 131 | 128 | 122 | 121 | 2 | 2 | 9 | 35 |
| Rb | 1031 | 1022 | 722 | 398 | 371 | 875 | 42 | 45 | 124 | 22 |
| Sr | 57 | 55 | 34 | 26 | 26 | 32 | 12 | 12 | 26 | 29 |
| Pb | 62 | 65 | 95 | 66 | 63 | 53 | 26 | 23 | 21 | 27 |
| Zr | 224 | 224 | 206 | 229 | 237 | 182 | 349 | 289 | 395 | 292 |
| Nb | 30 | 31 | 24 | 24 | 28 | 27 | 46 | 37 | 30 | 43 |
| Y | 169 | 166 | 131 | 130 | 143 | 82 | 107 | 83 | 212 | 81 |
| Ce | 152 | 137 | 149 | 48 | 28 | 87 | 53 | 33 | 147 | 84 |
| Sc | 1.2 | 1.2 | 1.0 | 0.9 | 0.9 | 0.9 | 1.0 | 1.0 | 1.1 | 0.8 |
| V | 2 | 2 | 8 | 5 | 6 | 8 | 14 | 19 | 6 | 32 |
| Cr | 1.2 | 1.2 | 4.0 | 1.8 | 3.7 | 0.9 | 4.0 | 5.8 | 1.1 | 55.8 |
| Ni | 1.2 | 4.8 | 1.0 | 0.9 | 0.9 | 0.9 | 2.0 | 1.9 | 1.1 | 60.6 |
| Cu | 1.2 | 12.1 | 9.9 | 14.7 | 14.8 | 17.1 | 42.4 | 42.7 | 12.8 | 30.3 |
| Zn | 70 | 80 | 52 | 68 | 67 | 66 | 55 | 58 | 66 | 62 |
| Field No | MJ8 | MJ10 | MJ6 | MJ7 | MJ9 | MJ11 | MJ3 | MJ5 | MJ13 | MJ15 |

FIGURE 6

**Graphed Geochemistry
(mass per unit volume basis)**





Tin Geochemistry

In order to resolve any doubts, Sn analyses were carried out. If the kaolinised granites were the hydrothermal source of the tin mineralisation, then they would be expected to be markedly enriched in this metal in relation to the pink granite. The extent of enrichment would be expected to be several orders of magnitude. Tin in granites is typically 3-5 ppm, Sn in ore is about 5000 ppm (0.5%).

The results are tabulated below:-

| Rock Type | ppm | | | | mg/ml | | | |
|-----------------------|-----|----|----|----|-------|-----|-----|----|
| Clay Sediment | 40 | | | | 64 | | | |
| Debris Flow Sediments | 55 | 65 | 50 | | 111 | 126 | 107 | |
| Kaolinised Granite | 20 | 20 | 25 | 45 | 40 | 37 | 47 | 86 |
| Pink Granite | 15 | 15 | | | 37 | 36 | | |

If the Sn content of the kaolinised granite is expressed on a mass per unit volume basis then it is closely comparable to that of the pink granite. The debris flow sediments, and also possibly the clay, are slightly enriched in Sn, presumably due to gravity concentration. The Sn level in the granite is high but stanniferous granites in Malaysia carry some 60 ppm Sn compared to the normal granitic background of 3 ppm (Aranyakanon, 1972). The rest of the geochemistry of these granitic rocks indicates that they are highly differentiated (Chappell pers comm) and would consequently be expected to be enriched in some elements.

Thus it is concluded that the high background of Sn is related to the highly-differentiated and volatile-rich nature of the granite as a whole, which is why there is a tin-field there in the first place. The kaolinised granite is not enriched in Sn relative to the pink granite. There is, therefore, no compelling evidence at all to support hydrothermal kaolinisation at Trial Hill.

INTERPRETATION

Kaolinisation at Trial Hill

The history of kaolinisation of the granitic basement is complex at Trial Hill. The original hypothesis was that kaolinisation had accompanied hydrothermal alteration of the granites along narrow zones, accompanying Sn mineralisation in or about late Carboniferous times. This hypothesis has not withstood detailed investigation. Kaolinisation by weathering has clearly taken place to an appreciable depth below the pre-Pliocene lateritic surface. Uplift or tilting of the land surface rejuvenated the drainage, caused active

erosion and gave rise to the debris-flow and fluvial deposits. The old river bed, now filled with Pliocene gravels and debris, may have been aligned to an old joint feature, down which post-Carboniferous weathering had penetrated deeply. The sediments, filling the old river bed, contain a very large kaolinite component, stripped from the old land-surface, so vast quantities of kaolinite must have been present and readily available for erosion and sedimentation in the source region at that time. The debris-flow and fluvial sediments, and to a lesser extent, the regolith overlying the granite, were effective aquifers, so kaolinisation of the granite basement no doubt continued during Pliocene to recent times, as did kaolinisation and redistribution of iron in the overlying sediments. Petrographic and field evidence for this has been presented.

The sediments overlying the granite at Trial Hill are remarkably similar to the Pliocene Campaspe Beds. These consist of argillaceous, gritty sandstone, fine- to medium-grained sandstone and rare siltstone. They are regarded as piedmont deposits, derived from granite, and were laid down under probably arid, but occasionally torrential conditions (Wyatt *et al*, 1970). The lower flows of the Nulla Basalt has been shown to have followed and filled older river courses.

Very localised kaolinisation, probably also related to weathering, occurs adjacent to the black quartz veins in the granite. No field or other evidence for hydrothermal kaolinisation was seen in exposures of the pink granite available to this author at the Trial Hill Mine. This author is not convinced of the presence of a kaolinised funnel in the granite below the deposit. There is however ample evidence for kaolinisation by weathering during one and possibly two events. Silvery accordion structures of mixed kaolinite and muscovite, common as 'authigenic' minerals in saprolites of many kinds, were probably mistaken for the micas of a greisen.

While the project did not get off to a good start, in that field, petrographic and geochemical evidence were unable to support what we had, at first, been led to believe (that the samples were typical of hydrothermal kaolinisation), they instead provided an excellent opportunity to investigate alteration of muscovite to kaolinite and kaolinite to halloysite by weathering. A paper (Robertson and Eggleton, in press) has emerged from this weathering study. The author was also able to gain useful experience in understanding the fabrics of saprolites, which has assisted him in investigations with the AMIRA/CSIRO Yilgarn Gold Project (P240 and P241) of which RGC Exploration Pty. Ltd., is a sponsor.

ACKNOWLEDGEMENTS

The author wishes to acknowledge assistance by many of the expert staff at the Australian National University, where he learned numerous new techniques as a 'mature' student. In particular Jack Wasik for carrying out very reliable gravimetric determinations of some of the samples for H₂O and CO₂. He also instructed the author in these arts and in the determination of Fe²⁺. Dr. B.W. Chappell, R. Freeman and E.

Webber carried out high quality XRF analyses. N. Ware of the Research School of Earth Sciences provided expert help with the microprobe. J.S. Preston and R. Heady of the Forestry Department instructed the author in using the SEM. P.J. Barlow of the Research School of Chemistry assisted with the TEM. C. Foudoulis of the Geology Department helped with ion beam milling, X-ray diffraction analysis and photography. K.K. Cheeswright of CSIRO drafted Figure 1 and the cover. In particular the author is indebted to Dr. R.A. Eggleton for his guidance, instruction, enthusiasm and encouragement in, for the author, a very new field of research. RGC Exploration Pty. Ltd. made the visit to the Trial Hill Tin Mine possible and supplied logistics and accommodation while there. Kevin Robinson provided the initial samples and introduced me to the Trial Hill site. Eddie Harper (tin miner and poet) provided hospitality on site at Trial Hill. ARGS Grant E8115611R enabled the research to be carried out. All this is acknowledged with appreciation.

REFERENCES

- Aranyakanon, P. 1972. Geochemical studies of tin in granite and basalt and of fine tin alluvium, Thailand. In Proc. 2nd Seminar Geochem. Prosp. Methods and techniques. U.N. Min. Res. Serv.. Ser. No. 38., 199-202.
- Banfield, J.F. 1985. The mineralogy and chemistry of granite weathering. Unpubl. M.Sc. Thesis. Australian National University. 229p.
- Hey, M.H. 1954. A new review of the chlorites. Mineralogical Magazine 30(224) pp277-92.
- Hobbs, B.E. 1968. Recrystallisation of single crystals of quartz. Tectonophysics. 6(5). pp 353-401 .
- Hughes, T.C. and Hannaker, P. 1978. The determination of carbon and hydrogen in geological materials by thermal decomposition. Chemical Geology. 22 pp 331-339.
- Lenthall, D.H., McCarthy, T.S. and McIver, J.R. 1974. A computer program for the construction of stereo-pairs of the CMAS tetrahedron. Trans. Geol. Soc. S. Afr., 77, 201-206.
- Morrison-Smith, D.J., Patterson, M.S., and Hobbs, B.E. 1976. An electron microscope study of plastic deformation in single crystals of synthetic quartz. Tectonophysics. 33. pp 43-79.
- Norrish K., and Chappell, B.W. 1977. X-ray fluorescence spectrometry. In Zussman. J (Ed) Physical methods in determinative mineralogy. Academic Press, London. pp201-72.

- Norrish, K., and Hutton, T.J. 1969. An accurate X-ray spectrographic method for the analysis of a wide range of geological samples. *Geochimica et Cosmochimica Acta*. 33 p431 .
- Reineck, H.E., and Singh, I.B. 1980. *Depositional Sedimentary Environments*. Springer-Verlag, New York. 549 pp.
- Riley, J.P. 1958. Simultaneous determination of water and carbondioxide in rocks and minerals. *Analyst* (London). pp 44-49.
- Robertson, I.D.M., and Eggleton, R.A. (in press). The weathering of granitic muscovite to kaolinite and halloysite and plagioclase-derived kaolinite to halloysite. *Clays and Clay Minerals*.
- Wyatt, D.H., Paine, A.G.L., Clarke, D.E. and Harding, R.R. 1970. *Geology of the Townsville 1:250 000 Sheet Area, Queensland*. Bur. Miner. Resour. Aust. Rep. 127. 85 pp.